UNIVERSIDADE DE LISBOA

FACULDADE DE CIÊNCIAS

DEPARTAMENTO DE FÍSICA

Ultrasound Waveform Optimization for Power Efficient Focused Ultrasound Neuromodulation

Patrícia Monteiro Rodrigues

Mestrado em Engenharia Biomédica e Biofísica

Dissertação orientada por:

Guiomar Gaspar de Andrade Evans

Tiago Miguel Lopes Marta da Costa

2023

“Live as if you were to die tomorrow. Learn as if you were to live forever.”
— Mahatma Gandhi

Acknowledgments

First and foremost, I would like to express my deepest gratitude to my thesis supervisor, Dr. Tiago Costa, who gave me the opportunity to complete this internship and work in an exceptional team. I also want to thank him for always making me feel confident in my abilities and for providing an extremely good spirit in his group, TU MIND. Thank you for all the patience, constant guidance, and your smart and clear way of explaining physics. Thank you for everything, I was very lucky.

I also want to thank Professor Guiomar Evans, from the Faculty of Sciences of the University of Lisbon, for all the support during this year and for constantly wanting to know how I was doing and if I needed any help.

To all MSc and PhD students in the Bioelectronics department, I must express my appreciation for helping me and giving me the motivation and strength, I needed during these months. You quickly became my friends and made me feel at home, I am so grateful for everything. A special thanks to Gandhi, Hassan, and Cesc who guided me in this project and taught me so many things. I would also like to thank my dear MSc friends Niels and Matteo for making my time in Delft very pleasant and for providing me with help with all my questions and doubts.

I would like to thank my family for always supporting me and believing in me. Thank you, parents, for giving me the opportunity to have done this project abroad and for all the motivational calls I received. Thank you, sis, for never doubting me and making me stronger. I also want to thank my aunt Sandra and my cousins Tuta, Rapha, Sarah, and Joana for all their support.

I want to express my gratitude to all my friends, but a special thank you to my dear friends Alice, Ana, Padrela, Laura, Miguel, and Marco who helped me in very different ways, but they all gave me the support I needed.

Lastly, I want to thank my cute boyfriend Tiago for always believing in me and for being my biggest support during these months, and for all the motivation he gave me. For rising me up when I was sad and mad and for cooking dinner when I was late because I was finishing some measurements in the lab.

Abstract

Ultrasound neuromodulation is a promising ultrasound modality since it combines high spatial resolution and high coverage of the brain while remaining minimally invasive. It is performed by exciting a transducer with an alternating pulse signal at its resonance frequency. These pulse signals are typically sent in bursts. The piezoelectric transducer converts this signal into an acoustic wave, resulting in multiple acoustic waves within each burst. Bulk ceramic piezoelectric transducers have a high-quality factor, meaning that for a single pulse excitation, it produces several pulses with decaying amplitude.

The main goal of this dissertation was to explore potential power savings in the ultrasound transmitter by removing pulses from a long burst of pulses and bursts from the neuromodulation cycle while minimizing the decay of the acoustic wave amplitude. This goal was accomplished by developing an experimental setup for ultrasound stimulation using two different transducers: High-Intensity Focused Ultrasound and Air-Backing transducers. In this study, it was also simulated two different approaches: removing pulses by short and open circuits.

The results showed that using the Air-Backing transducer, it's possible to save more energy than with the other transducer. The simulations from the Air-Backing transducer, in which only a percentage of the pulse amplitude was removed, showed better results than the total removal of the pulses, and among the results presented, the 30% amplitude removal is the case with the highest efficiency.

Another comparison made in this project suggests that performing pulse removal through a short circuit generates very positive results while performing pulse removal through an open circuit was not beneficial to the hypothesis under study.

Future work to be done should include experiments and simulations with neurons since the behavior of ultrasound in neurons is still not fully understood, and the obtained results may prove to be quite different from the simulations.

Keywords: Ultrasound, Ultrasonic Neuromodulation, Noninvasive, Pulse Removal

Resumo

Os ultrassons (US) são ondas sonoras com frequências acima do limiar percetível da audição humana, que é aproximadamente 20 kHz. A resolução de uma imagem de ultrassom está relacionada com o comprimento de onda das ondas acústicas no tecido humano. A neuromodulação por ultrassons é uma técnica que pode substituir a estimulação cerebral profunda (DBS), uma vez que pode excitar e suprimir reversivelmente a atividade neuronal de uma forma não invasiva. Na DBS, são colocados elétrodos em regiões específicas do cérebro, e os impulsos elétricos são utilizados para ativar o tecido cerebral próximo, o que é altamente invasivo. Ao utilizar os ultrassons como a fonte portadora de energia para a neuromodulação, não é necessário implementar elétrodos no cérebro. Isto permite que o ultrassom seja utilizado como uma técnica de neuromodulação precisa, mas não invasiva. A utilização de ultrassons torna também possível combinar a neuromodulação com as técnicas de obtenção de imagens comumente utilizadas. A neuromodulação por ultrassons tem muitas vantagens uma vez que pode fornecer uma enorme quantidade de informação sobre uma determinada doença localizada no cérebro.

O principal objetivo deste projeto de dissertação é o desenvolvimento de uma configuração experimental de estimulação por ultrassons e posterior investigação dos efeitos da remoção de impulsos de uma onda acústica na energia final da mesma. A principal característica deste estudo foi a remoção de pulsos completos das ondas de ultrassom ou a sua remoção parcial, ou seja, a redução da amplitude de uma certa percentagem de pulsos em vez apenas da remoção completa do pulso. Assim, será possível analisar os efeitos destas diferenças nas ondas de ultrassons, principalmente em termos de diferença de potencial e pressão. Estas simulações de remoção de pulsos foram realizadas com diferentes transdutores (um transdutor de ultrassons focado de alta intensidade e um transdutor com uma caixa de ar) para analisar e concluir qual deles permitiria a obtenção de melhores resultados. Para além da comparação descrita, foi realizada uma comparação entre a remoção de pulsos por um método de curto-circuito ou circuito aberto para compreender qual deles é mais eficaz.

A metodologia para este estudo consistiu primeiramente na elaboração de um código que permitisse a simulação de uma onda de ultrassom e onde fosse possível remover pulsos da mesma, através do software MATLAB. Posteriormente, para adquirir as imagens de ondas de ultrassom desejadas, foi preparada uma montagem experimental inicial constituída por diversos equipamentos, entre eles, um tanque de água. Assim, primeiramente encheu-se o tanque com água destilada, uma vez que a velocidade do ultrassom na água é semelhante à velocidade do ultrassom em tecidos moles (corpo humano). Um transdutor de 2,8 mm x 2,8 mm foi utilizado para simular as alterações no perfil do feixe quando as ondas foram removidas. O transdutor utilizado era constituído por um PZT (zirconato de chumbo titanato) montado num circuito integrado de silício. À sua frente, colocámos um hidrofone de agulha de 0,5 mm, um microfone concebido para ser utilizado debaixo de água e para gravar som. O hidrofone foi ligado a um acoplador DC (corrente contínua) com fonte de alimentação que serve como acoplador de sinal acústico entre o pré-amplificador submersível e o sistema de medição e que também fornece o sinal de alimentação DC ao pré-amplificador. O hidrofone foi inserido num sistema de posicionamento de três eixos controlado por uma unidade de controlo. O próprio acoplador DC foi ligado a um osciloscópio que permite observar e analisar a forma dos sinais aplicados, gerados por um gerador de sinais, capaz de gerar diferentes tipos de formas de ondas elétricas.

À última configuração, foram feitas algumas alterações. O tanque de água foi instalado em cima de uma mesa ótica. Uma mesa ótica é uma mesa única que absorve todas as vibrações do ambiente circundante e proporciona um ambiente livre de vibrações, não causando assim qualquer tipo de erro relacionado

com as vibrações externas e permitindo medições de alta precisão. Foram utilizados 2 transdutores diferentes para realizar as medições, um transdutor focado de alta intensidade e um transdutor que possuía uma caixa de ar.

A aquisição de dados iniciou-se com a transmissão do respetivo código MATLAB para o gerador de sinais, com a indicação do sinal a ser gerado. De seguida o transdutor recebeu o sinal proveniente do gerador e começou a emitir ondas de ultrassons. O hidrofone captou as ondas enviadas pelo transdutor e reencaminhou os sinais para o osciloscópio. Utilizando uma interface gráfica de utilizador (GUI), denominada Experiment Visual Acoustics (EVA), extraiu-se os parâmetros do sinal, e foi possível analisá-los. O valor máximo da pressão em todas as diferentes simulações foi traçado e analisado.

Na experiência anterior, cada vez que um pulso era retirado da onda, o PZT era ligado à massa, provocando muitos curtos-circuitos. Em vez de um curto-circuito, o objetivo era ter um circuito aberto sempre que se desejasse remover um pulso. A fim de conseguir um circuito aberto, como desejado, foi projetado um circuito e desenhada a respetiva Placa de Circuito Impresso (PCB).

Posto isto, todos os dados foram adquiridos e analisados de igual forma. Os sinais foram extraídos para o MATLAB e foram obtidos os envelopes da parte superior dos mesmos. Por último, os envelopes de cada sinal controlo e de cada sinal não controlo (sinal com percentagem de pulsos removidos) foram sobrepostos a fim de comparar os mesmos e calcular o percentual de energia perdida.

Neste estudo, investigou-se se é possível poupar energia durante a neuromodulação ultrassónica, através da remoção de pulsos da onda de ultrassom ou através da redução da sua amplitude. Os resultados sugerem que alguma energia pode ser poupada através da remoção de pulsos de ondas acústicas.

Ao utilizar o transdutor com a caixa de ar, os resultados foram mais promissores e eficazes. Ao remover cerca de 20% da energia, a perda expetável seria de 20%, no entanto apenas se perde cerca de 7%, o que representa uma poupança considerável de energia. Por outro lado, o transdutor de ultrassons focado de alta intensidade não foi tão eficaz, perdendo em cada simulação quase toda a percentagem de energia expetável.

No que diz respeito aos resultados do transdutor com caixa de ar foi tirada outra conclusão muito favorável à hipótese colocada; as simulações, em que apenas uma percentagem da amplitude do pulso foi removida, mostraram melhores resultados do que a remoção total dos pulsos, e entre os resultados apresentados, a remoção de 30% da amplitude é o caso com a menor percentagem de perda e, portanto, a maior eficiência.

Outra comparação feita neste projeto sugere que a realização da remoção de pulsos através de um curto-circuito gera resultados muito positivos, enquanto a realização da remoção de pulsos através de um circuito aberto não foi benéfica para a hipótese em estudo, não tendo sido obtidos resultados favoráveis. É de notar que todos estes resultados implicaram alguns erros de medição, no entanto, as conclusões foram claras e corroboradas umas pelas outras.

Este estudo lança uma nova luz sobre a utilização de ultrassons para o tratamento de doenças neuronais, abrindo várias possibilidades inovadoras de investigação, podendo assim contribuir para a evolução, e desenvolvimento da neuromodulação ultrassónica de uma forma mais fiável e prática, tornando possível a execução deste método através de equipamentos com baterias recarregáveis que proporcionam ao

utilizador uma terapia vinte e quatros horas por dia ao invés das terapias existentes atualmente que só podem ser feitas no hospital.

Apesar dos resultados obtidos neste estudo, este possui ainda algumas limitações associadas principalmente a erros de medição. Em primeiro lugar, todos os resultados deveriam ter tido um tamanho de amostra maior, a fim de terem uma melhor análise estatística. Outra coisa importante seria reduzir os erros de medição, por exemplo, utilizando comprimentos de cabo mais curtos e utilizando a mesa ótica desde a primeira instância.

O trabalho futuro a ser feito deve incluir experiências e simulações com neurónios, quer em ratos, quer em células vivas, uma vez que o comportamento do ultrassom nos neurónios é desconhecido e os resultados podem revelar-se bastante diferentes, pelo que é crucial a realização destas experiências. Algo a considerar é também utilizar transdutores com um fator de qualidade mais elevado e assegurar que a simulação é realizada exatamente na frequência de ressonância, uma vez que é possível alcançar a máxima potência de ultrassons e um menor consumo de energia com um fator de qualidade elevado.

Palavras-Chave: Ultrassons, Neuromodulação Ultrassónica, Não Invasivo, Remoção de Pulso

List of Figures

List of Tables

List of Abbreviations

US – Ultrasound

DBS – Deep Brain Stimulation

TMS – Transcranial Magnetic Stimulation

DCS – Direct Current Stimulation

FUS – Focused Ultrasound

LIFU – Low-Intensity Focused Ultrasound

HIFU – High-Intensity Focused Ultrasound

LILFU – Low-Intensity Low-Frequency Ultrasound

CNS – Central Nervous System

PRF – Pulse Repetition Frequency

PW – Pulse Width

SD – Sonication Duration

ISPPA – Spatial-peak Pulse-averaged Intensity

ISPBA – Spatial-peak Burst-averaged Intensity

ISPTA – Spatial-peak Temporal-averaged Intensity

MI – Mechanical Index

PZT – Lead Zirconate Titanate

PML – Perfectly Matched Layer

AD – Alzheimer´s Disease

PD – Parkinson's Disease

PML – Perfectly Matched Layer

RMS – Root Mean Square

GUI – Graphical User Interface

PECVD – Plasma Enhanced Chemical Vapor Deposition

PCB – Printed Circuit Board

Contents

1 Introduction

Ultrasounds (US) are sound waves with frequencies higher than the upper perceptible restriction of human hearing, roughly 20 kHz. The resolution of an US image is related to the wavelength of the acoustic waves in tissues. It is a form of energy that quickly penetrates soft tissues at wavelengths on the order of 1.00 mm, ranging from $0.3 < \lambda < 3$ mm [1], [2]. In medicine, it is used both for diagnostic and therapeutic applications. The typical frequencies range for the medical US is from $1 \sim 15$ MHz. It is used in diagnostics to build an image of internal body structures, including tendons, muscles, joints, blood vessels, and internal organs, quantify specific properties (such as distances and velocities), and provide an informative auditory sound. Its goal is usually to locate a disease source or rule out pathology [1], [3].

Ultrasounds can modify the behavior of the human brain. Ultrasound neuromodulation is a technique that could replace deep brain stimulation (DBS) since it can excite and reversibly suppress neuronal activity in a non-invasive way. In DBS, electrodes are placed into particular regions of the brain, and electrical pulses are used to activate the nearby brain tissue, which is highly invasive [4], [5]. Using ultrasound as the energy carrier for neuromodulation, no implanted electrodes are needed. This allows ultrasound to be used as a precise, but noninvasive neuromodulation modality. The use of ultrasound also makes it possible to combine neuromodulation with US imaging. Ultrasound Neuromodulation has a lot of advantages since it combines high spatial resolution (on the order of the wavelength of the driving frequency) and high coverage of the brain while remaining minimally invasive (any desired depth) [1], [3].

Non-invasive methods capable of treating some psychiatric and neurologic disorders are highly needed. The two more established non-invasive techniques are transcranial magnetic stimulation (TMS) and transcranial direct current stimulation (tDCS). TMS uses rapidly changing magnetic fields to stimulate the brain. The magnetic fields induce currents that can cause action potentials in the neurons. This technique has been demonstrated to be effective in treating depression and severe headaches. tDCS uses direct electrical currents to stimulate areas of the brain. Two electrodes are placed over the head, and a steady, low-intensity current flows through them, modulating neural activity [6]–[8]. However, these techniques have a considerable problem based on their limited spatial targeting and low penetration depth [9].

Developments in ultrasound transducer technology have generated highly focused ultrasound (FUS) fields. There are two types of focused, therapeutic ultrasound: low-intensity focused ultrasound (LIFU), 0.125 – 3 Wcm^{-2}, and high-intensity focused ultrasound (HIFU), 5 Wcm^{-2}. HIFU is used essentially for tissue ablation, mainly through coagulation necrosis. On the other hand, LIFU is commonly used to stimulate the neurons to treat injuries. This technique can suppress neuronal activity without any brain damage [10], [11]. LIFU uses low frequencies once the acoustic waves need to pass through the skull with as less absorption, reflection, and scattering as possible. It is proven that those phenomena are prevalent at higher frequencies (1 to 15 MHz) than at lower frequencies [12].

Ultrasound neuromodulation is performed by exciting a piezoelectric transducer with an alternating voltage at its resonance frequency, ranging from the hundreds of Hz up to 10 MHz. This alternating voltage is typically sent in bursts, with typical burst durations ranging from hundreds of microseconds

to a few milliseconds, burst repetition frequency from hundreds of Hz to a few kHz, and a total neuromodulation cycle often in the order of seconds. The piezoelectric transducer converts this alternating voltage into a corresponding acoustic wave. Altogether, this results in hundreds to thousands of acoustic waves within each burst, and to hundreds to thousands of bursts within a neuromodulation cycle.

Bulk ceramic piezoelectric transducers have a high-quality factor, meaning that for a single pulse excitation it produces several acoustic pulses with decaying amplitude. The main goal of this dissertation was to explore potential power savings in the ultrasound transmitter, by removing pulses from within the long burst of alternating voltages, and bursts from within the neuromodulation cycle, while minimizing the decay of the acoustic wave amplitude. This has the potential to reduce the power consumption of ultrasound neuromodulation systems towards efficient battery power operation.

The main feature of this study will be the removal of complete pulses from the ultrasound waves or their partial removal, i.e., reducing the amplitude of a certain percentage of pulses rather than removing them completely. Thus, it will be possible to analyze the effects of these differences in the ultrasound waves, mainly in terms of voltage and pressure. These pulse removal simulations will be performed with different transducers (a high-intensity focused ultrasound transducer and an air-backing transducer) to analyze and conclude which one gives better results. After comparing the two transducers, a comparison between removing pulses by short circuit or open circuit will also be performed to understand which is more effective.

With this study, the world is one step closer to creating wearable devices capable of performing neurostimulation with ultrasound. The fact that these devices are portable is really important since we can have 24/7 treatment for better stimulation and better results. It is also important for the patient to have a normal life and not have the worry of being near a plug in case of a seizure (for example, epilepsy seizures).

Translated with www.DeepL.com/Translator (free version)This manuscript is divided into 6 chapters. The first chapter is the introduction, then the theoretical background necessary to understand this work is introduced in chapter 2. The 3rd chapter has the methodology, where it is explained all the instrumentation setups used in this study, the programs explored as well as all the techniques put into practice. The results of this study are presented in chapter 4 and discussed in chapter 5. General conclusions, contributions, and further work are provided in chapter 6.

2 Background

This chapter consists of a literature review where some studies and techniques already developed in this area of Ultrasound Neuromodulation are described. Some topics such as ultrasound mechanisms, ultrasound parameters, and potential treatments will be discussed.

2.1 ULTRASOUND NEUROMODULATION MECHANISMS

US Neuromodulation mechanisms are poorly understood, but a few possible tools explain how US neuromodulation works (**Figure 2.1)**. One of the possible mechanisms is mechanosensitive ion channel modulation. William J., Tyler, et al. found that low-intensity low-frequency US (LILFU) stimulates the opening of the Na+ channels; therefore, it increased the sodium conductance through the hippocampal neurons, and they also observed Ca^{2+} transients in response to the ultrasound neuromodulation [4].

Sangjin Yoo1, David R. Mittelstein et al. [9] also discovered that ultrasound neuromodulation predominantly activates the primary rodent's cortical neurons in culture through a mechanical mechanism mediated by calcium-selective mechanosensitive ion channels that causes the opening of some ion channels, including TRPP1/2, TRPC1, and Piezo1 (a large mechanosensitive ion channel protein). When these channels are activated, calcium builds up gradually, which is amplified by calcium and voltage-gated channels, resulting in a burst firing response.

Jan Kubanek, Jingyi Shi et al. have seen in vitro that the ion channels TREK-1, TREK-2, and TRAAK were also sensitive to ultrasound waves [13]. Other studies and experiments showed *in vitro* that both Piezo1 and Piezo2 were also sensitive to US stimulation [14]–[16]. Another possible mechanism is thermal modulation. Ultrasound absorption by tissues could result in a rise in temperature once the energy of the ultrasound is converted into heat. Thus, the temperature rise depends on many factors, such as tissue properties, US parameters, beam configuration and scanning configuration [17]. The rising temperature is proven to change the membrane capacitance, conductance, and action potentials, resulting in depolarization [18]–[20].

The intramembrane cavitation model is the response to the mechanism of US neuromodulation in some studies [21]. Cavitation means the formation of tiny bubbles in a liquid. The US can cause a complicated mechanoelectrical interplay that leads to excitation, owing to currents produced by membrane capacitance changes (**Figure 2.1)**.

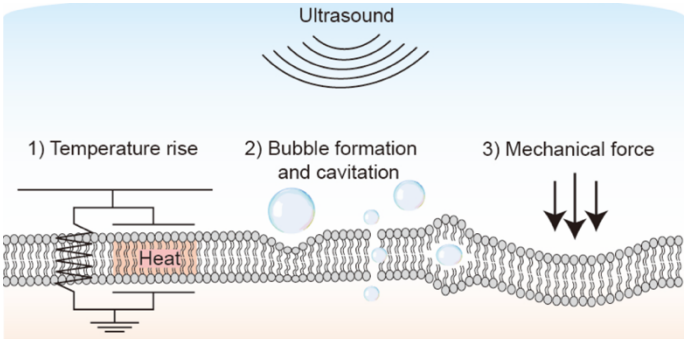

Figure 2.1*- Potential biophysical effects of ultrasound neuromodulation. The figure is taken from* [9]

Michael Plaksin et al. [21] explained the fundamentals of Central Nervous System (CNS) acoustic stimulation and predicted how stimulation parameters affect the empirically reported efficacy of mouse motor cortex ultrasonic stimulation [21]. **Table 2.1** summarizes some of the ultrasonic neuromodulation mechanisms.

***Table 2.1**- Summary of potential mechanisms associated with ultrasound neuromodulation. Table adapted from the paper of Hermes Kamimura* [16]

Mechanisms	Description
Membrane deformation causing capacitance changes	Capacitance changes were seen during artificial membrane deflection, deformation of in vitro membranes, membrane volume changes, and flexoelectric effect.
Soliton model	Changes in membrane conformation could arise from interfering with a thermodynamic process involved in electromechanical pulse traveling during action potentials.
Intramembrane cavitation model	Ultrasound-induced intramembrane cavitation within the bilayer membrane induces a current through membrane capacitance changes.
Mechanosensitive ion channel modulation	Several mechanosensitive ion channels were seen in vitro to be sensitive to ultrasound waves.
Modulation of TRPA1 channels in astrocytes	Ultrasound opens TRPA1 channels in astrocytes, inducing glutamate-releasing as a mediator of glia-neuron interaction.
Thermal modulation	Heating reversibly alters the membrane capacitance, resulting in depolarization. Focused Ultrasound can increase the temperature at specific regimes. Neuronal membrane conductance and synaptic potentials are altered by temperature changes.

2.2 ULTRASOUND PARAMETERS

In the past decades, ultrasound has been thoroughly researched in the field of diagnostic imaging. However, studies on ultrasound stimulation of the nervous system are sparse, leaving room for numerous future investigations. The development of technology and medical science has made ultrasound neuromodulation an increasingly important field of research. The ultrasound parameters are essential since they could change the efficacy of neuronal stimulation. There is a good quantity of different studies where several ultrasound parameters were used and tested both in humans and animals (mice, rats, sheep, macaques, ovine, and swine).

Figure 2.2 represents a typical waveform of ultrasounds with some of the most critical parameters. The acoustic waves are defined by the period (T), and the amplitude of the acoustic wave represents the intensity. Even though US spatial resolution is a component of the acoustic frequency, in the brain, spatial resolution can be modeled as acoustic wavelength, **equation 2.1**. The λ is the wavelength, c represents the sound velocity, and f is the frequency.

$$\lambda = \frac{c}{f} \qquad (2.1)$$

The frequency of the waves affects the spatial targeting of the brain regions, and higher values produce tighter focus neurostimulation [22]. The pulse repetition frequency (PRF) determines the rate at which acoustic pulses are delivered; The duty cycle (DC) dictates the proportion of each pulse filled with cycles of ultrasound at the fundamental frequency. It is calculated by multiplying the pulse width (PW) by the PRF. The sonication duration (SD) is defined as the total time from the beginning of the first pulse to the end of the last pulse. It is proven that longer durations favor the inhibition of cortical neurons, whereas short durations produce excitation.

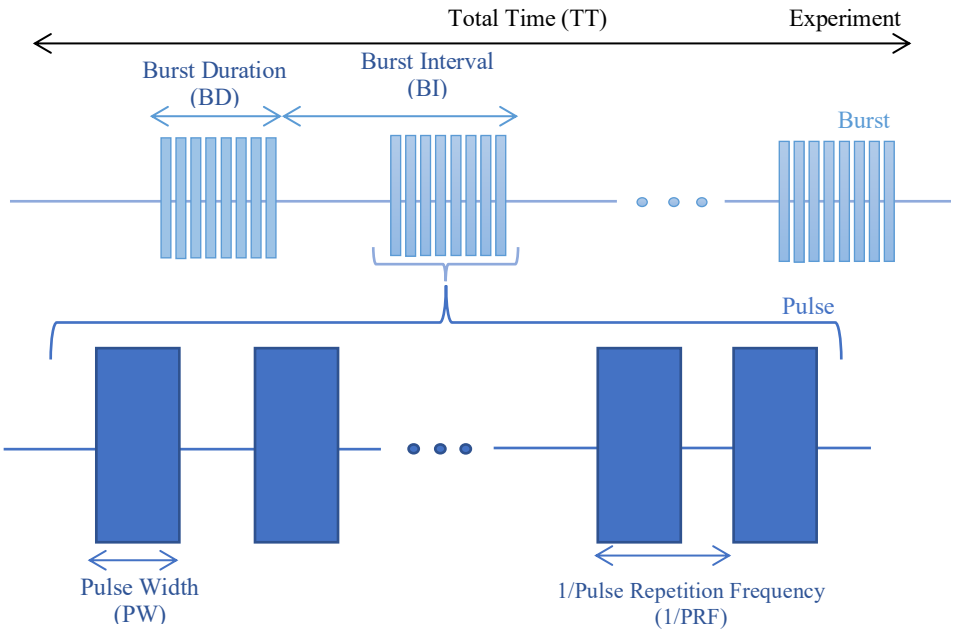

Figure 2.2 - *Typical waveform of ultrasounds with some important parameters. The light blue part represents the burst, and the dark blue part represents the pulse.*

There are three most essential intensities in an ultrasound burst: the spatial-peak pulse-averaged intensity (I_{SPPA}), the spatial-peak burst-averaged intensity (I_{SPBA}), and the spatial-peak temporal-averaged intensity (I_{SPTA}). The I_{SPBA} represents the intensity averaged over one single burst. The I_{SPTA} is the intensity averaged over the experiment's total duration, proportional to SD. The I_{SPPA} is defined as the average intensity of a single pulse, and it can predict and estimate short-term mechanical-biological effects [22]–[25].

To estimate destructive mechanical-biological effects it is calculated the Mechanical Index (MI), which is a tool that is defined as negative peak pressure divided by the square root of the frequency of the ultrasound wave. The outstanding value of the MI should be <1.9 to avoid bioeffects, such as inertial cavitation (occurs when the bubble diameter grows to at least twice its original diameter). In order not to cause brain damage, Food and Drugs Administration (FDA) guidelines consider a maximum safety value of $I_{SPTA} < 720$ mW/cm^2 and $I_{SPPA} < 190$ W/cm^2 [3].

In **Tables 2.2** to **Table 2.5**, there are summarized some ultrasound neuromodulation experiences of both animals and humans' studies using ultrasound in different parts of the brain.

Table 2.2- *Ultrasound neuromodulation experiences: resume of animals' studies using ultrasound neuromodulation in different parts of the brain - Part 1*

Study	Animal	Brain Target	Sonication parameters	Findings
[26]	Mice	Motor Cortex	**Frequency** = 500 kHz **I_{SPPA}** = 0.8 W/cm^2 **PRF** = 1 kHz **SD** = 400 ms **DC** = 40 %	Ultrasound pulses induced motor response, neural activity, and rapid hemodynamic response selectively at the stimulation site.
[27]	Rabbit	Motor Cortex	**Frequency**: 0.68 MHz **I_{SPPA}**: 12.6 W/cm^2 **I_{SPTA}** = 6.3 W/cm^2 **PRF**: 10 Hz **SD**: 1 s	Motor activity was elicited. The minimum intensity required to elicit excitatory effects was 1.6 W/cm^2 I_{SPTA} (3.3 W/cm^2 I_{SPPA}). No brain damage was found in any animals.
[28]	Rat	Hippocampus	**Frequency**: 2.5 MHz **I_{SPPA}**: 9.8 W/cm^2 **I_{SPTA}**: 7.84 *m*W/cm^2 **PRF**: 500 Hz **SD**: 160 ms **PD**: 1.6 ms	Low-intensity US modulated gamma oscillations in the rat hippocampus, as well as altered low-frequency phase-locked gamma amplitude differences and the couplings between the delta, theta, alpha, and gamma oscillations were enhanced by FUS.
[29]	Mice	Somatosensory Barrel Cortex	**Frequency** = 350 kHz **PRF** = 2.0 kHz **DC** = 42.8 % **SD** = 0.5 ms	Ultrasound neurostimulation-induced depolarization of pyramidal cells.
[30]	Rat	Thalamus	**Frequency**: 0.65 MHz **I_{SPPA}**: 6 W/cm^2 **PRF**: 0.1 kHz **Duty cycle**: 5 % **SD**: 20 min	Decreased recovery time from anesthesia through indication with behavior and physiological changes.

Table 2.3 *- Ultrasound neuromodulation experiences: resume of animals' studies using ultrasound neuromodulation in different parts of the brain - Part 2*

Study	Animal	Brain Target	Sonication parameters	Findings
[31]	Mice	Somatosensory Area	**Frequency**: 2 MHz **I_{SPPA}**: 46 W/cm^2 **I_{SPTA}**: 0.7 W/cm^2 **PRF**: 1000 Hz **Duty cycle**: 30 % **SD**: 300 ms	Ultrasound modulation elicited head-turning in mice generating a significantly larger number of head-turning responses compared to control (0.78 compared to 0.22 of normalized responses).
[4]	Mouse (brain slices)	Hippocampus	**Frequency**: 0.44 MHz **I_{SPPA}**: 2.9 W/cm^2 **I_{SPTA}**: 0.023 W/cm^2 **PRF**: 0-100 Hz **PD**: 30 µs	Very low intensity US was demonstrated to be capable of eliciting SNARE proteins-mediated exocytosis and synaptic transmission in hippocampal circuits. No damage was found.
[32]	Mice	Motor cortex Retrosplenial cortex Somatosensory Cortex Posterior parietal Visual Cortex Auditory cortex	**Frequency**: 2 MHz **Intensity:** 97 W/cm^2 **PRF**: 1000 Hz **Duty cycle**: 50 % **SD**: 300 s	US stimulation elicits spatially specific motor responses, therefore the large neural volume including the subcortex contains many neural circuits all with their own complex excitation and inhibition mechanism to US.
[33]	Mice	Motor Cortex	**Frequency**: 0.183 MHz **I_{SPPA}:** 0 - 530 mW/cm2 **I_{SPTA}:** 0 - 47.4 mW/cm2 **PRF:** 200 Hz **Duty cycle**: 90 % **SD**: 200 s	Modulation was observed at a 100% success rate over 10 trials in free moving mice. No damage was found.
[34]	Sheep	SM1, V1	**Frequency**: 0.25 MHz **I_{SPPA}**: 0.5- 14.3 W/cm^2 **PRF**: 500 Hz **Duty cycle**: 50 % **PD**: 1 ms **SD**: 300 ms	US elicits motor responses over a certain intensity threshold which varies substantially across the animals tested with intensities greater than 6 W/cm^2 it was supposed to excite motor and visual cortex potentials. Most animals showed no damage present, however a **few microhemorrhages were noted** when sonication was given repetitively.

Table 2.4 *- Ultrasound neuromodulation experiences: resume of humans' studies using ultrasound neuromodulation in different parts of the brain- Part 1*

Study	Subject	Objective	Brain Target	Sonication parameters	Findings
[35]	Human	Chronic disorders of consciousness	Thalamus	**Frequency**: 0.65 MHz **I_{SPTA}**: 720 mW/cm^2 **PRF**: 100 Hz **PD**: 0.5 ms **SD**: 30 s	LIFUP patient emerged from disorder of consciousness, however it is uncertain whether the observed effects are causally linked to the LIFUP sonication or whether the patient spontaneously, and serendipitously, emerged from a Disorder of Consciousness.
[36]	Human	How US inhibit somatosensory potentials	Thalamus	**Frequency**: 0.5 MHz **I_{SPPA}**: 7.03 W/cm^2 **PRF**: 1000 Hz **Duty cycle**: 36 % **PD**: 0.36 ms **SD**: 500 ms	US inhibited somatosensory evoked potential with latencies between 14 and 21 ms and inhibited the early negativity around 35 ms. Furthermore, **decreased gamma power and attenuation as well as alpha and beta amplitude** in some EEG channels.
[37]	Human	Modulate mood in healthy human	Right Prefrontal Cortex	**Frequency**: 500 kHz **I_{SPTA}**: 130 mW/cm^2 **PRF**: 40 Hz **Duty cycle**: 0.26 % **PD**: 30 s **SD**: 65 μs	30-s FUS induced positive mood effects for up to 30 min. 2 min of tEUS modulated functional connectivity related to the Right Prefrontal Cortex and Default Mode Network.
[38]	Human	How different parameters influence the motor cortex of healthy subjects	Primary Motor Cortex (M1)	**Frequency**: 500 kHz **I_{SPTA}**: 0.93/2.78/4.63 W/cm^2 **PRF**: 1000 Hz **Duty cycle**: 10/30/50 % **SD**: 0.1 – 0.5 s	Inhibitory effect. Ultrasound dose-dependently suppressed TMS-elicited motor evoked potentials. Decreased reaction time on visuomotor tasks.
[39]	Human	How US affects mental states	Posterior Frontal Cortex	**Frequency**: 8 MHz **I_{SPTA}**: 0.152 W/cm^2 **SD**: 15 s	Improvement in subjective mood 10 min and 40 min after Transcranial Ultrasound compared to placebo.

Table 2.5 *- Ultrasound neuromodulation experiences: resume of humans' studies using ultrasound neuromodulation in different parts of the brain - Part 2*

Study	Subject	Objective	Brain Target	Sonication parameters	Findings
[40]	Human	Influence of US on sensory tasks	Primary Somatosensory Cortex (S1)	**Frequency**: 0.5 MHz **I_{SPPA}**: 5.9 mW/cm^2 **PRF**: 1 kHz **Duty cycle**: 36 % **SD**: 500 ms	Attenuation of the amplitudes of somatosensory evoked potentials elicited by median nerve stimulation. Enhancement of performance on sensory discrimination tasks. The sonication elicited transient tactile sensations on the hand area.
[41]	Human	Examine the effects of a diagnostic tUS device on cortical excitability	Primary Motor Cortex (M1)	**Frequency**: 2.32 MHz **I_{SPPA}**: 34.96 W/cm^2 **I_{SPTA}**: 132.85 mW/cm^2 **Duty cycle**: <1 %	Stimulation resulted in a local and distal decrease in blood-oxygen-level dependent signal in the affected left globus pallidus (GP) and in large-scale cortical networks, as well as a general decrease in relative perfusion throughout the cerebrum after sonication.
[42]	Human	Influence of FUS sonication of the primary visual cortex in healthy humans	Primary Visual Cortex (V1)	**Frequency**: 270 kHz **I_{SPPA}**: 0.7-6.6 W/cm^2 **PRF**: 500 Hz **Duty cycle**: 50 % **SD**: 300 ms	Elicited blood-oxygen-level dependent signal, phosphene perception and distinct electroencephalogram peaks.
[43]	Human	Using Low-intensity focused ultrasound to modulate left basal ganglia structures in healthy volunteers	Left Lateralized Basal Ganglia Structures	**Frequency**: 650 kHz **I_{SPTA}**: 720 mW/cm2 **I_{SPPA}**: 14.40 W/cm2 **Duty cycle**: 5 % Two sets of parameters: (1) **PD** :0.5 ms; **PRF:** 100 Hz (2) **PD**: 5 ms; **PRF**: 10 Hz	Ultrasound inhibits the amplitude of single pulse Motor evoked potentials and attenuates intracortical facilitation but does not affect intracortical inhibition. Ultrasound also reduces reaction time on a simple stimulus response task.

2.3 POTENTIAL APPLICATIONS OF NEUROMODULATION

Neuronal diseases are a huge concern worldwide since they are numerous, and the causes behind them remain unknown. Those diseases are characterized by the early and gradual loss of neurons in some central nervous system regions (CNS). They include epilepsy, psychiatric disorders, and neurodegenerative diseases. **Figure 2.3** represents the different targets for US neuromodulation in the treatment of neurological diseases.

In general, all ages worldwide are affected by neurological and psychiatric illnesses, which affect close to a billion people worldwide. 0.5% to 1% of the world's population suffers from epilepsy, characterized by recurring seizures. A 3.8% prevalence of people suffer from depression worldwide, and around 2 to 3% of people have Obsessive-compulsive disorders (OCD), which shows up as obsessions and recurrent behaviors [44]–[46].

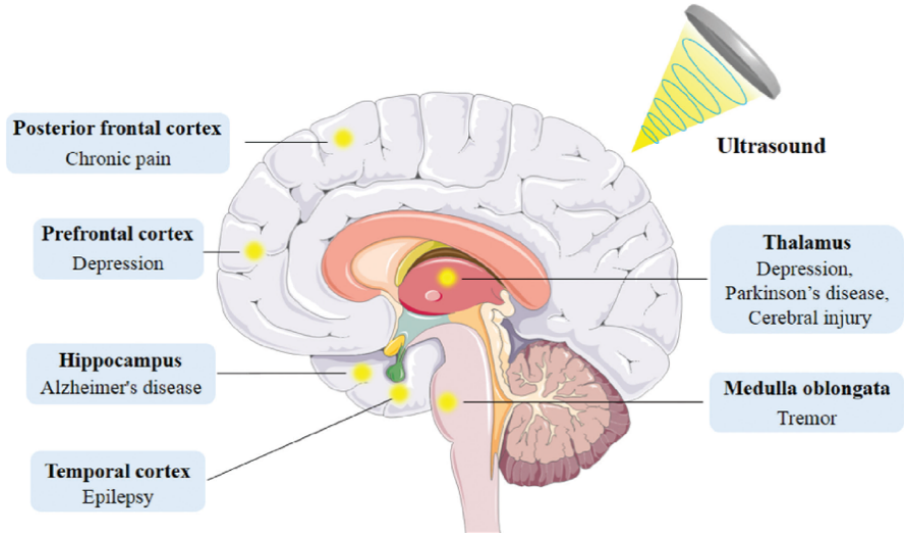

Figure 2.3 *- Image that represents targets for ultrasonic neuromodulation in the treatment of neurological diseases. The thalamus, medulla oblongata, and temporal lobe of the human brain might all be stimulated by ultrasound to treat a variety of neurological conditions such as Alzheimer's disease, depression, epilepsy, and tremor.* [47]

2.3.1. Most Common Diseases and Treatments

Epilepsy is a common disease that affects the brain, and it is characterized by recurrent seizures. Seizures can be described as bursts of electrical activity in the brain that affects its activity temporarily. Usually, it appears either in children or people over sixty years old, and it is lifelong, although the symptoms can get better over time [48]. Anti-epileptic medications can reduce neuronal activity and help prevent seizures. Nevertheless, they do not treat epilepsy. When there are no significant neurological adverse effects, surgical excision of the epileptic area may potentially be an option. Neurostimulation (DBS and TMS) has been shown to decrease the number of seizures in some patients [49], [50].

Alzheimer´s Disease (AD) is a disorder that slowly destroys the neurons in the brain, making the person lose memory and the ability to do simple and daily tasks. Often, the first symptoms appear later in life [51]. Although some medications can halt the progression of AD by controlling the activity of

neurotransmitters, there is currently no known treatment. It is crucial to understand the AD cause in order to research directions for curing or preventing AD.

Depression is directly linked to environmental and genetic variables. Its mechanism suggests a neurotransmitter imbalance, especially an excess of the stress hormone cortisol [52]. Antidepressants can be used to reduce the symptoms of depression, although they have significant side effects such as nausea, insomnia, fatigue, and weight gain [53]. Although, depression can be treated with electroconvulsive therapy and neurostimulation (DBS, TMS, tDCS) [54]–[56]. Nowadays, Korea is the only country in the world that use US neuromodulation as a tool to treat depression.

Parkinson's Disease (PD) is a brain condition that results in unintentional or uncontrollable movements like trembling, stiffness, and issues with balance and coordination [57]. When the first symptoms appear, almost 80% of the neurons have already died. Analogous to AD, there is no known cause of PD, and there is no cure for PD. Usually, patients take some medication that helps with the symptoms. Nowadays, neuromodulation is also used to improve the patient's condition. DBS has been proven to reduce motor symptoms. However, since it is strongly invasive, it is only used in severe cases, where drugs are ineffective [58], [59].

2.4 NEUROMODULATION IN MICE

Ultrasound neuromodulation is usually done in mice to see its efficacy and the short and long-term secondary effects before being used in humans. These studies make it possible to characterize, validate, and optimize the mechanical and biological results due to brain neuromodulation [60].

Nowadays, most of all, the equipment capable of doing neuromodulation in animals, especially in mice, is huge, and it requires anesthesia which can inhibit neural activity [61], [62]. It becomes unsuitable to do the necessary experiments associated with perception, cognition, and behavior. Therefore, a head-mounted ultrasound stimulator was already designed and fabricated for inducing neuromodulation in awake mice [31].

The typical setup used in ultrasound neuromodulation in mice is illustrated in **Figure 2.4**. It has an electrophysiological recorder, a function signal generator, a power amplifier, and an ultrasound transducer. The mice can be anesthetized with different types of anesthesia, such as sodium pentobarbital, ketamine, xylazine, and telazol. All anesthesia is supposed to last the whole experiment.

Different studies have proven the efficiency of ultrasound neuromodulation in mice, and they have used different values of the parameters of the acoustic waveform.

There is a preparation before executing the stimulation in mice. It all starts with the weighting of the mouse to calculate the anesthesia needed and inject it. Afterwards, all the hair from the scalp and limbs is removed, and the head fix is positioned on the mouse. The next step is to implant limb electrodes and to apply acoustic gel to transmit the signal better. After this process ends, it is time to do the focused ultrasound.

The center transducer is placed over the origin of the navigation using a pulse-echo scan and repositioned to the desired brain region, defining the grid of targets. This process is repeated until any sign of consciousness [32].

It is necessary to choose the waveform parameters before starting the stimulation. Christian Aurup, Hermes Kamumira et al. [32] in an experiment used a fundamental frequency of 2 MHz, a pressure of 1.76 MPa, an ISPPA of 97 W/cm^2, a pulse duration of 0.5ms, a PRF of 1 kHz, a Duty cycle of 50 %, and a sonication duration of 300 ms. The brain region they wanted to stimulate was the motor region, including most of the motor cortex, the retrosplenial cortex, the somatosensory cortex, the posterior parietal, the visual cortex, and the auditory cortex.

They concluded that different target regions exhibit different responses to US neurostimulation and have different intensity thresholds to elicit a response. They also observed that no cumulative effect from successive stimuli indicated the lack of thermal mechanisms driving these responses.

In another experiment, H. Kim, S. Kim et al. [33] used different parameters of the ultrasound wave. They tried a frequency of 0.183 MHz, an ISPPA between 0 and 530 mW/cm^2, an ISPTA between 0 and 47.4 mW/cm^2, a PRF of 200 Hz, a duty cycle of 90 %, a sonication duration of 200 ms, and a pulse duration of 0.5 ms. The brain region they wanted to stimulate was the motor cortex.

They conclude that, with less than half of the frequency used by Christian Aurup, Hermes Kamumira et al. [32] the neuromodulation was observed at a 100% success rate over ten trials, and there was no damage found.

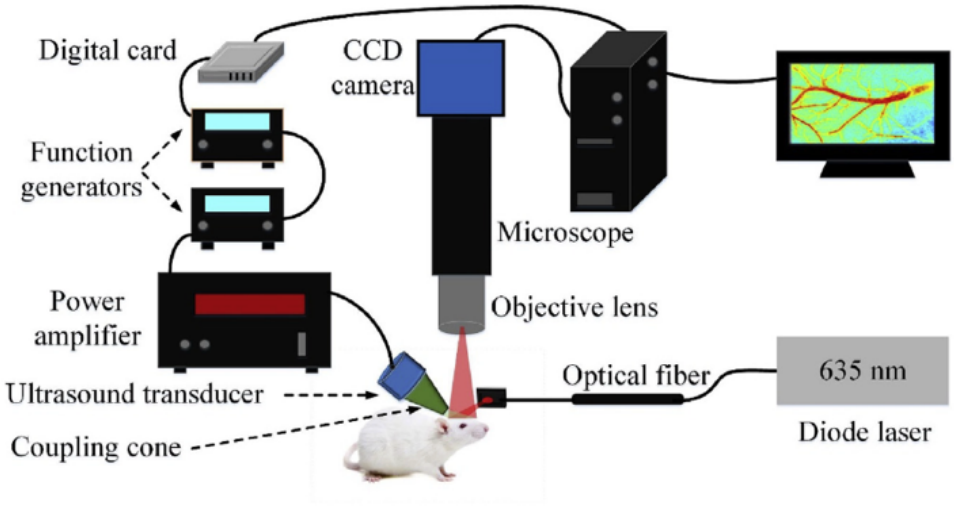

Figure 2.4 *- Example of an experimental setup in ultrasound neuromodulation in mice. There are function generators that create the signal and send it to the Ultrasound transducer and Diode that generate laser radiation through a semiconductor. The figure is taken from* [63]

2.5 SAFETY OF US MODULATION

As mentioned above, the ideal ultrasound neuromodulation technique should be non-invasive and should precisely target the brain circuits, both deep and superficial.

Only two studies reported brain damage from all the studies and experiments analyzed using ultrasound neuromodulation. W. Lee, S. D. Lee, et al. [34] reported adverse effects of microhemorrhages in sheep, and W. Legon, L. Ai, et al. [40] saw some mild negative symptoms in humans, as can be seen from **Table 2.4** and **Table 2.5**, shown above.

Around the fundamental frequency of 650 kHz, ultrasound neuromodulation is safe. When using high intensities of neuromodulation, it is necessary to be very cautious once high frequencies can cause irreversible brain damage such as apoptosis, necrosis, or vascular damage due to its thermal effects [34], [40], [64].

2.6 TISSUES PROPERTIES

The typical value used by the scientific community for the sound velocity of soft tissue is 1540 m/s, although each tissue has its own sound velocity since it is dependent on the physical properties of tissue, such as tissue resistance, density, and elasticity [65].

The acoustic impedance of tissue is an important property when it comes to medical ultrasound imaging since the differences in impedance between two tissues are used to obtain echoes of ultrasound waves. Acoustic impedance, Z [Rayls], refers to the reflection or transmission characteristics of tissue and it is calculated by multiplying ρ the tissue´s mass density [kg/m^3] and c the speed of sound within the tissue [m/s], **equation 2.2**:

$$Z = \rho c \tag{2.2}$$

Even though the characteristics of the human tissue are relatively similar, there are notable reflections at the boundary between the two materials. This is explained by the fact that small variations in medium properties can result in huge reflections, as is explained in the definition of the reflection coefficient, **equation 2.3**:

$$R = \frac{Z_2 - Z_1}{Z_2 + Z_1} \tag{2.3}$$

Where R means the dimensionless reflection coefficient and Z_1, Z_2 the acoustic impedance of two adjacent tissue types.

Table 2.6- *Examples of density, velocity, and acoustic impedance on different tissues and materials. Data were taken from* [2], [66], [67]

Material/Tissue	**ρ [kg/m^3]**	**c [m/s]**	**Z [MRayls]**
Kidney	1037	1561	1.62
Blood	1060	1584	1.68
Liver	1058	1608	1.65
Bone	1990	3198	6.36
Brain	1035	1562	1.62
Fat	928	1430	1.33
Muscle	1041	1580	1.66
Water	1200	1540	1.48
Air	1	343	0.0003

2.7 TRANSDUCER

2.7.1. Transducer's Components

A transducer is an electronic device that converts a signal in one form of energy to a signal in another form[66]. In US neuromodulation, this device is needed to transmit pulses since it can convert electrical signals into sound waves and back (**Figure 2.5)**.

The quality factor "Q" of a transducer describes the width of the frequency range to which the ceramic element(s) ring when current is applied to the transducer. It is true that maximum ultrasonic power is achieved when a transducer with a high Q factor is operated exactly at its resonant frequency. High Q-factor transducers are commonly used in Doppler ultrasound applications, and they also have advantages in ultrasonic cleaning applications due to their relatively low power consumption [68]. Mathematically, the Q factor is the operating frequency divided by the bandwidth, **equation 2.4**.

$$Q = \frac{Frequency\ (MHz)}{Bandwidth\ (MHz)} \tag{2.4}$$

A piezoelectric material is the most used material on a transducer for ultrasound devices. The piezoelectric effect is known as the voltage or electrical potential that will appear across the sides of the piezoelectric material when it is subjected to mechanical stress. In other words, it is the conversion of mechanical waves into electrical waves. This effect is reversible in that the direct piezoelectric effect can be reversed to generate mechanical stress via the application of an electrical charge [67].

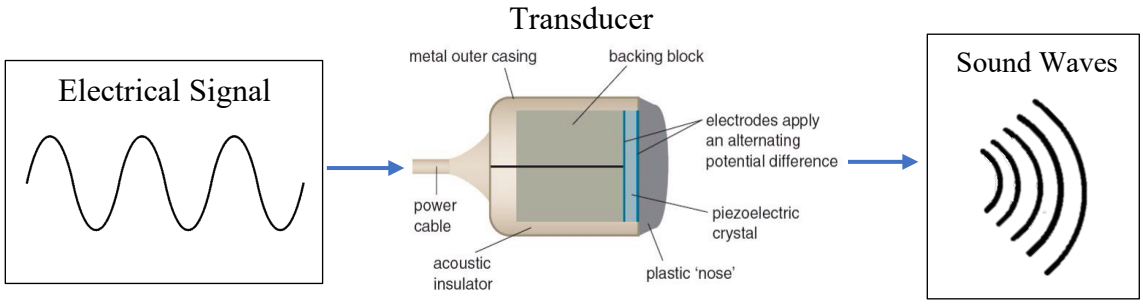

Figure 2.5 *- Flowchart of the normal behavior of an ultrasonic transducer. It converts an electrical signal into sound waves receiving their echoes back.*

The efficiency with which a piezoelectric material transforms electrical energy into mechanical energy or vice-versa is measured by the electromechanical coupling factor, $k_{ij,}$ **equation 2.5**. The direction in which the electrical field is applied is indicated by the first subscript "*i"*, while the second subscript "*j*" indicates the direction in which the mechanical energy is applied[69].

$$k_{ij} = \sqrt{\frac{\pi}{2}\frac{f_r}{f_a}\tan\left(\frac{\pi}{2}\frac{f_a - f_r}{f_a}\right)} \tag{2.5}$$

In **equation 2.5**, the resonance and anti-resonance frequencies (occurs when the inertial force generated by the levered mass cancels the spring force) are denoted by the letters *fr* and *fa*. Increasing *k* can significantly increase the sensitivity and bandwidth of ultrasonic transducers [70].

Lead zirconate titanate (PZT) is the ultrasound transducer's most commonly used piezoelectric material due to its strong piezoelectric property, including a high electromechanical coupling factor [71].

2.7.2. Potential Energy Savings

The development of battery-powered wearable ultrasonic stimulators is severely constrained by the average power needed to produce the whole acoustic waveform, which is currently in the region of 1-10 W and proportional to the number of pulses.

This project is based on the hypothesis that the probability of eliciting an action potential won't decrease if a specific number of pulses are removed from the acoustic waveform. The basis for this is that the dynamics of neuronal activation are much slower (around 1 millisecond) than the duration of a single acoustic pulse (around 1 microsecond), so the absence of a given number of acoustic pulses would have a negligible effect on successful stimulations [72]. Since the transducer has a resonant action, it will continue to vibrate and generate ultrasounds even if a pulse is not sent every now and then. This might lead to a more energy-efficient way of stimulating neurons.

Thus, by removing some pulses from a burst or even decreasing the amplitude of some pulses, it is idealized that some energy can be saved.

2.8 FINAL ULTRASOUND REMARKS

This introduction summarized some of the studies that have been done in the ultrasound neuromodulation field.

It has been shown that ultrasounds can modulate neural activity in both the central and peripheral nervous systems in cell cultures, hippocampal slices, small animals, large animals, and humans. All the data collected suggest that the potential to enhance or suppress nerve firing depends on the US parameters.

The US parameters that the community agree to be ideal for stimulation are a PRF ranging from 500 to 1500 Hz and a DC of around 50-70%. Whereas, for suppression, a PRF of less than 100 Hz and a DC of about 10% were the best. The central frequency could be up to 2.9 MHz, in animals, since it can still generate motor responses; greater than 2.9 MHz requires a sonication with much more intensity[36]. In humans, the most used frequencies range is between 250 kHz and 500 kHz[34], [40], [42]

However, parameters like the intensity and the sonication duration depend strongly, not only on the target region of the brain that must be stimulated or inhibited but also on the type and quantity of anesthesia administrated so, because of that, further research is required to find the optimum parameters when considering those factors.

In conclusion, the US is emerging as a non-invasive method that modulates brain activity safely. It can understand normal brain function and for diagnostic and therapeutic applications in diseases such as Parkinson’s or epilepsy. However, when the intensities are higher, more damage is reported. As a result, when following the FDA's US standards, it's safe to believe that US neuromodulation is a safe procedure, but many mechanistic questions remain to be answered.

3 Methods

In this chapter, the materials and methods used in this project are precisely described. Firstly, there is an explanation of how the ultrasound waves were created and how pulses were removed. Then, it is discussed how the assemblies of both the short and open circuits are done, and it is explained for each case how the data was obtained and later analyzed.

3.1 ULTRASOUND MATLAB CODE

3.1.1 Beam Profile Creation

An ultrasound wave with some bursts was created using the k-wave Toolbox, running on MATLAB R2021b (MATLAB and K-wave Toolbox Version 1.3 Release 2020; The MathWorks, Inc., Natick, MA). To check if removing some pulses of a burst influences the beam profile of the ultrasound wave, a source of ultrasound was created on a computational grid with a perfectly matched layer (PML) inside, **Figure 3.1**. A PML is an artificial layer that absorbs the outgoing waves from the interior of a computational region without reflecting them into the interior. The PML size was twenty grid points on the *x*-axis and ten on the *y* and z-axis. The number of grid points in the *x* direction was sixty-four and in both the *y* and *z* directions was seventy-four.

The grid point spacing in all directions was 0.05 mm. The time array was created using *kgrid.t_array,* and the time spacing in the time array was 0.01 μs. The properties of the propagation medium were defined: the sound speed as 1540 m/s and the sound density as 1200 kg/m^3. Three sensors on the *x*, *y*, and *z*-axes were also created to receive the waves produced by the source. The sensors were positioned almost in the middle of the computational grid in each plane to be near the focal spot, **Figure 3.2**.

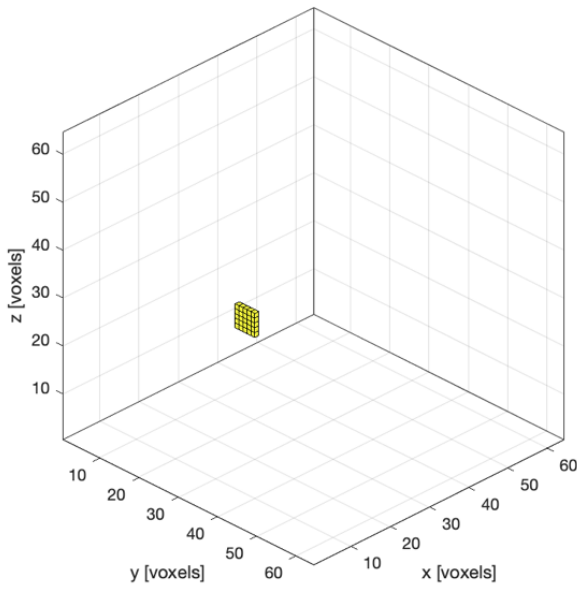

Figure 3.1 *- Source of ultrasound waves created on MATLAB, using the k-wave toolbox*

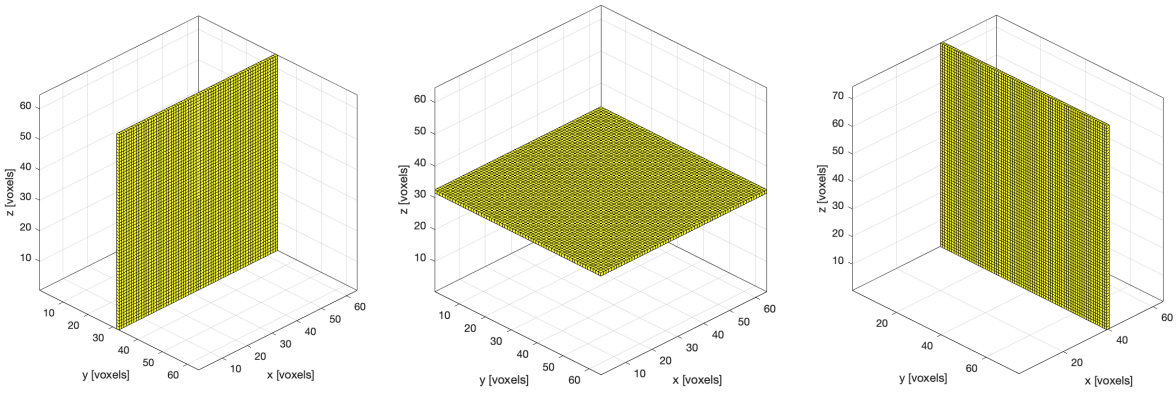

Figure 3.2 - *Sensors created on MATLAB on the different planes. Left: plane XZ; Middle: plane XY; Right: plane YZ.*

The wave's frequency was defined as 5 MHz, and the period of the wave was defined as the inverse of the frequency. The time-varying sinusoidal source was then created using the function *sin* of MATLAB. Random numbers were created inside a *for* loop; if the random numbers were bigger than 0.9, the sinusoidal wave was set to zero. With this loop, waves were removed with a probability of 10%, **Figure 3.3**.

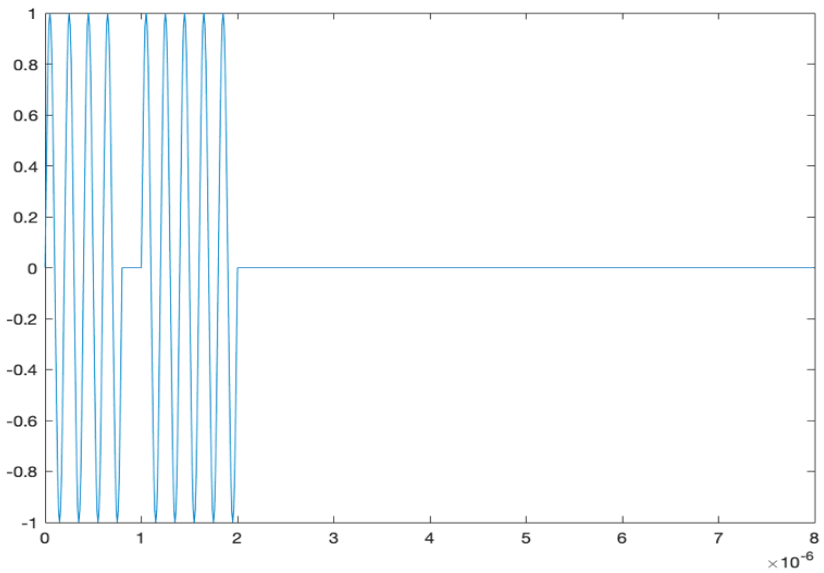

Figure 3.3 - *Simulation of a waveform with ten pulses, where one was removed.*

Using the root mean square (RMS) of the pressure, it was possible to create the beam profile of the wave and realize if there were differences when some waves were removed, or if the amplitude of some waves was lower.

3.1.1 Measurement Setup for the Acoustic Wave Removal Simulation

To acquire the desired ultrasound wave images, a setup was assembled using a set of equipment, **Figure 3.4**.

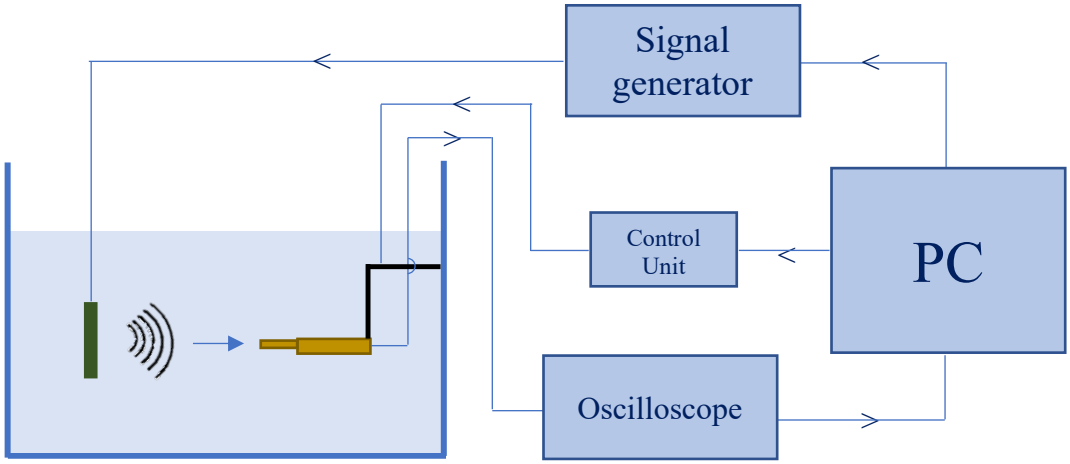

Figure 3.4 - *Connections between the equipment in the setup. The computer sends the waves generated on the software MATLAB to the transducer and the hydrophone captures the ultrasound waves and send them back to the oscilloscope. The oscilloscope is connected to the computer and using a GUI named EVA we can save the ultrasound images.*

We filled the tank with distilled water since the speed of the ultrasound in water is similar to the speed of the ultrasound in soft tissues (human body). A 2.8 mm x 2.8 mm transducer made in the laboratory was used to simulate the changes on the beam profile when waves were removed. The transducer was made by a small PZT mounted on a silicon chip, **Figure 3.5**.

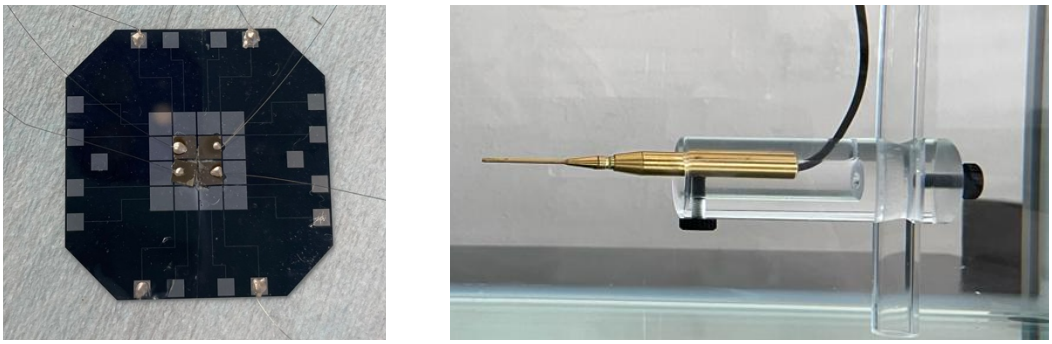

Figure 3.5 - *Left: 2.8 mm x 2.8 mm PZT on a silicon wafer transducer. Right: 0.5 mm needle hydrophone used to receive the waves sent by the transducer.*

In front of it, we put the 0.5 mm needle hydrophone (Precision Acoustics Ltd, Dorchester, United Kingdom), a microphone designed to be used underwater and record sound. The hydrophone was connected to the DC Coupler with Power Supply (Precision Acoustics Ltd, Dorchester, United Kingdom) which serves as an acoustic signal coupler between the submersible preamplifier and the user's measurement system and supplies dc power to the preamplifier. The hydrophone was inserted in a three-axis positioning system which was controlled by the Control Unit SFS630 (GAMPT Ultrasonic Solutions, Germany). The DC Coupler itself was connected to the Oscilloscope Agilent DSo 3032a (Agilent Technologies, InfiniiVision, California, United States) which displays and analyzes the waveform of electronic signals. The oscilloscope was connected to the Waveform Generator Rigol DG4202 (RIGOL Technologies EU, Gilching, Germany) which generates different types of electrical waveforms. The setup is shown in **Figure 3.6,** and the connections between the equipment are represented in the chart of **Figure 3.4**.

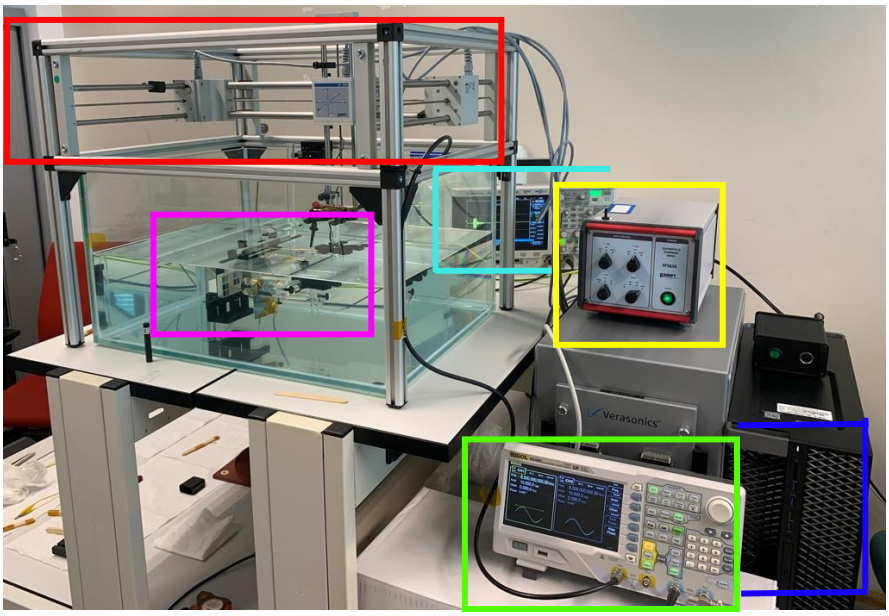

Figure 3.6 - *An overview photo of the experimental Setup. a) Red, top left: three-axis positioning system; b) Pink, center left: hydrophone; c) Light, blue center: oscilloscope; d) Yellow, center right: control unit; e) Green, bottom right: signal generator and f) Dark Blue, bottom right: Computer*

After the assembly was done, we started acquiring data. First, we sent the MATLAB code to the signal generator, where the wave was sent to the transducer, and it started emitting waves. The hydrophone received the ultrasound waves sent by the transducer, and it forwarded their data to the oscilloscope. Using a graphical user interface (GUI) named Experiment Visual Acoustics (EVA -Figure A1 from the appendix), we extracted the waveform data, and we could finally analyze it. The maximum value of the pressure in all the different simulations was plotted and compared.

3.2 EXPERIMENTAL SETUP SHORT CIRCUIT

Some alterations were made, to the last setup. The water tank was installed on top of an optical table. An optical table is a unique table that absorbs all the vibrations from the surrounding environment and provides a vibration-free environment, therefore not causing any type of error related to vibrations and letting high-precision measurements be done [72].

Some measurements were done using two different transducers: a 2.8 mm x 2.8 mm Air-Backing Unfocused transducer with a quality factor of 2,6, custom-made at TU Delft in another project, and a High-Intensity Focused Ultrasound transducer (HIFU), with a quality factor of 1,7.

The Air-Backing Transducer is shown in **Figure 3.7**. In that Figure, it is possible to see that the transducer is made of different materials, and it required different techniques. Between the glass and the silicon layer, there are some empty spaces filled with air.

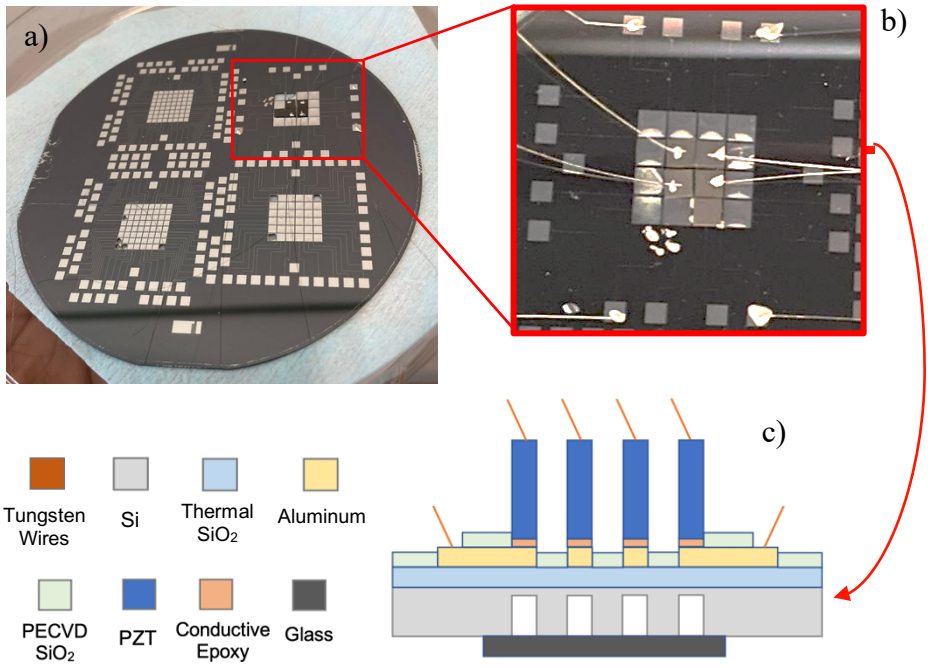

Figure 3.7 - *a) Top left: Custom made Air-backing transducer, made at TU Delft in another project, with multiple number arrays. b) Top right: Air-backing 4 x 4 array transducer. c) Bottom: Cross section of the 4 x 4 array transducer. In this image, it is possible to see all the components that the transducer is made of. The main component is PZT.*

The high-intensity focused ultrasound transducer (Precision Acoustics Ltd, Dorchester, United Kingdom) has a center frequency of 5 MHz, a focal length of 15 mm, and a 6 dB focal diameter of 350 µm. The internal impedance of this transducer is defined as 50 Ω and a 1.5-meter co-axial cable (BNC terminated) is attached to the transducer. In **Figure 3.8** it is possible to see the installation of the HIFU transducer on the water tank above the optical table.

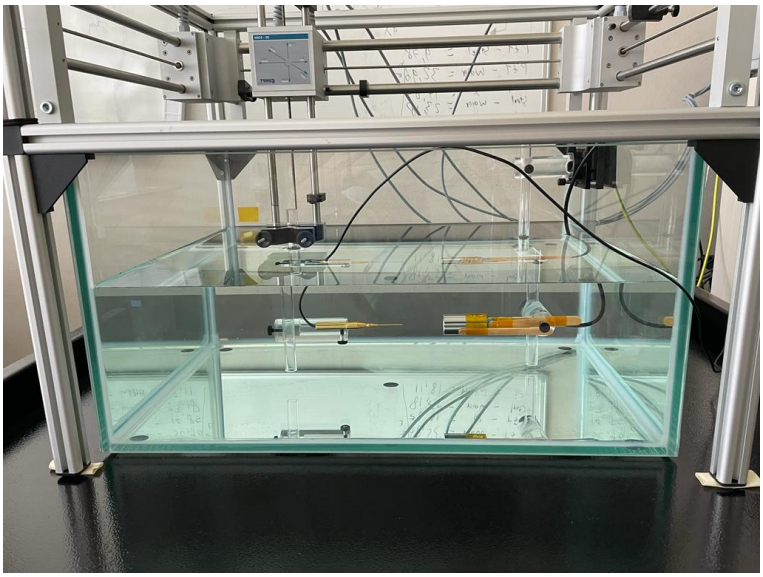

Figure 3.8 - *High intensity focused ultrasound transducer installed on the water tank. The hydrophone is positioned in front of it and the tank is on top of the optical table.*

After the assembly of all the setups, the measurements were done. As explained before, the MATLAB code was sent to the signal generator, where some pulses out of a waveform were removed. The ultrasound waves were captured by the hydrophone and, with the oscilloscope it was possible to analyze them.

After acquiring the data, the electrical interference from the wave was removed, and all the waves' first point was at the same time point and ended with the same data point as well. Thus, it was possible to be sure that the same amount of data was being compared. Before every measurement, where waves were removed, a control wave (without removing any wave) was performed, in order to reduce the measurement errors caused by the possible deviations of waves from each other, thus not having all the same size.

Having all the waveforms with the same amount of data points, starting at the same time and ending at the same time, the next step was converting the voltage into pressure. This was achieved by dividing the voltage waveforms by the hydrophone sensitivity, which is $1{,}352 \times 10^{-6}$ V/Pa. In **Figure 3.9** on the left, it is possible to see one example of an acquired control wave from the air-backing transducer after removing the electrical magnetic interference expressed in volts over time, and on the right, the same control wave expressed by pressure over time is illustrated. **Figure 3.10** represents the plot of the waveforms where two waves have been removed from the air-backing transducer; on the left, the wave is expressed in volts over time, and on the right, the wave represents pressure over time.

In **Figure 3.11** on the left, it is possible to see one example of an acquired control wave from the HIFU transducer after removing the electrical magnetic interference expressed in volts over time, and on the right, the same control wave expressed by pressure over time is depicted. Finally, **Figure 3.12** represents the plots of the waveforms where two waves have been removed from the HIFU transducer. As before, on the left, the wave is expressed in volts over time, and on the right, the wave represents pressure over time.

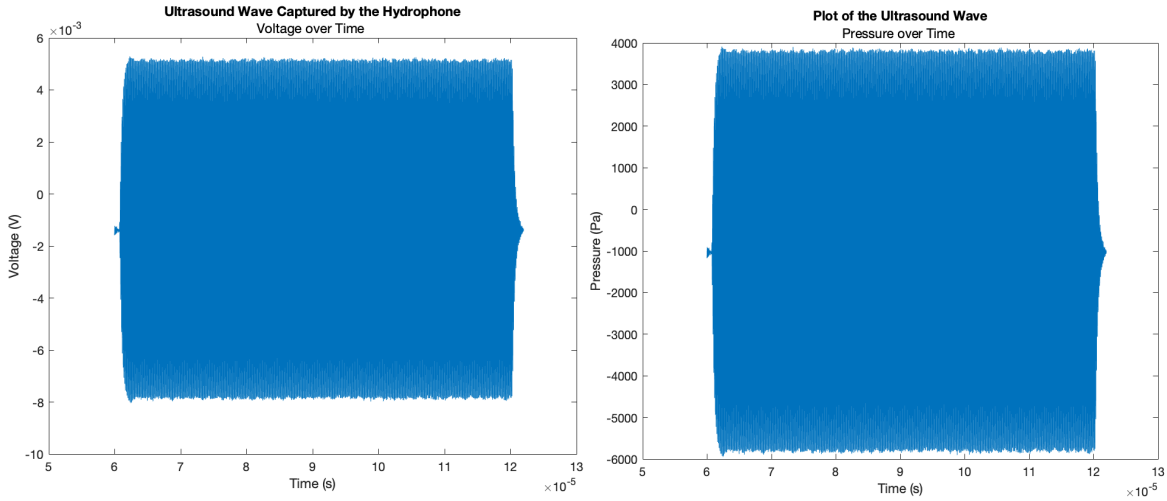

Figure 3.9 - *Ultrasound Wave sent by the Air-Backing transducer and captured by the hydrophone, after removing the electrical magnetic interference. On the left, there is one example of a control wave expressed in volts over time, and on the right, there is the same wave expressed in Mega Pascal over time.*

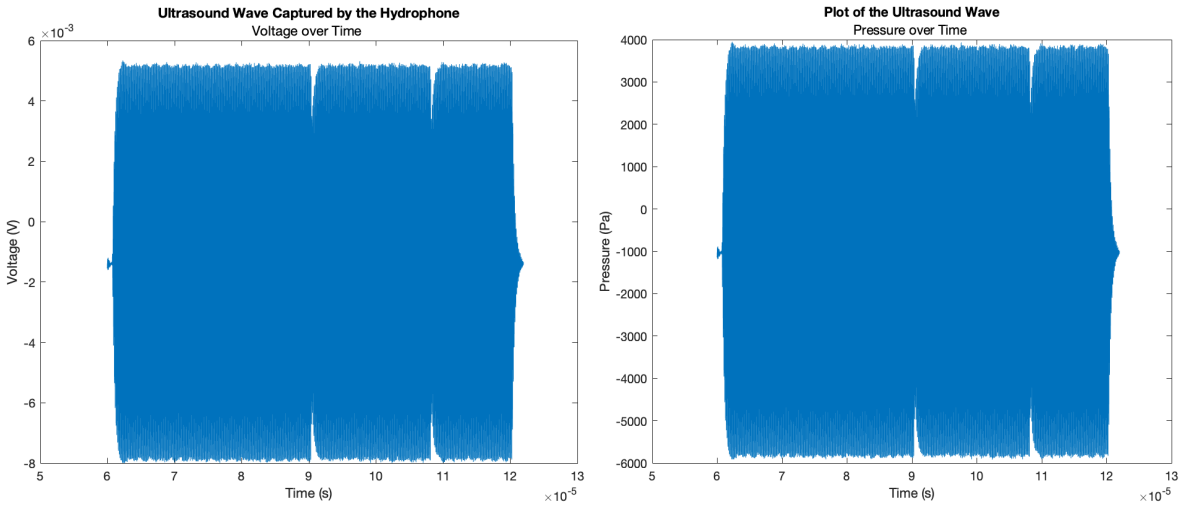

Figure 3.10 - *Ultrasound Wave sent by the Air-Backing transducer and captured by the hydrophone, after removing the electrical magnetic interference. On the left, there is a wave where two pulses have been removed, expressed in volts over time, and on the right, there is the same wave expressed in Mega Pascal over time.*

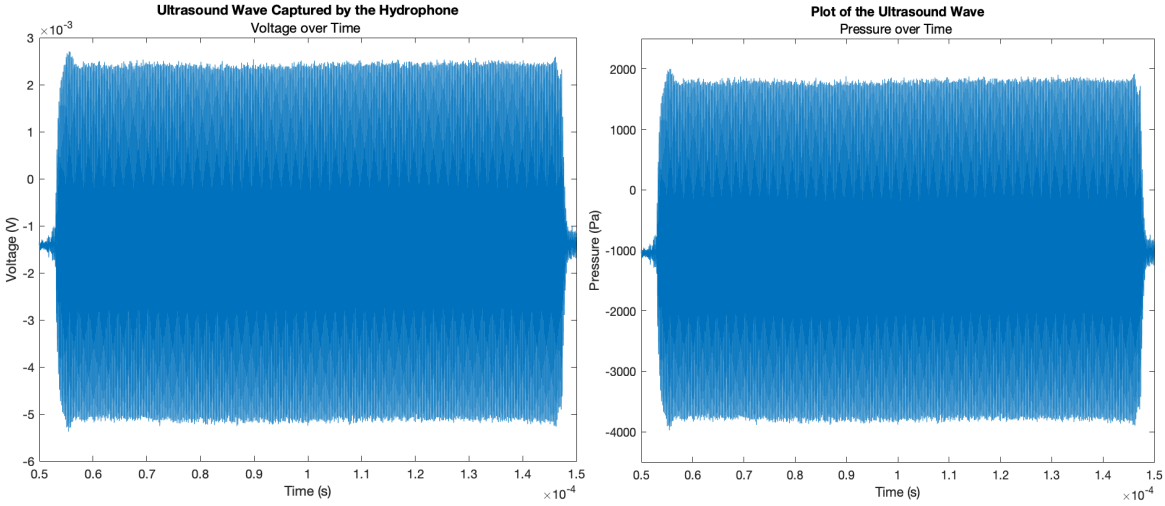

Figure 3.11 - *Ultrasound Wave sent by the HIFU transducer and captured by the hydrophone, after removing the electrical magnetic interference. On the left, there is one example of a control wave expressed in volts over time, and on the right, there is the same wave expressed in Mega Pascal over time.*

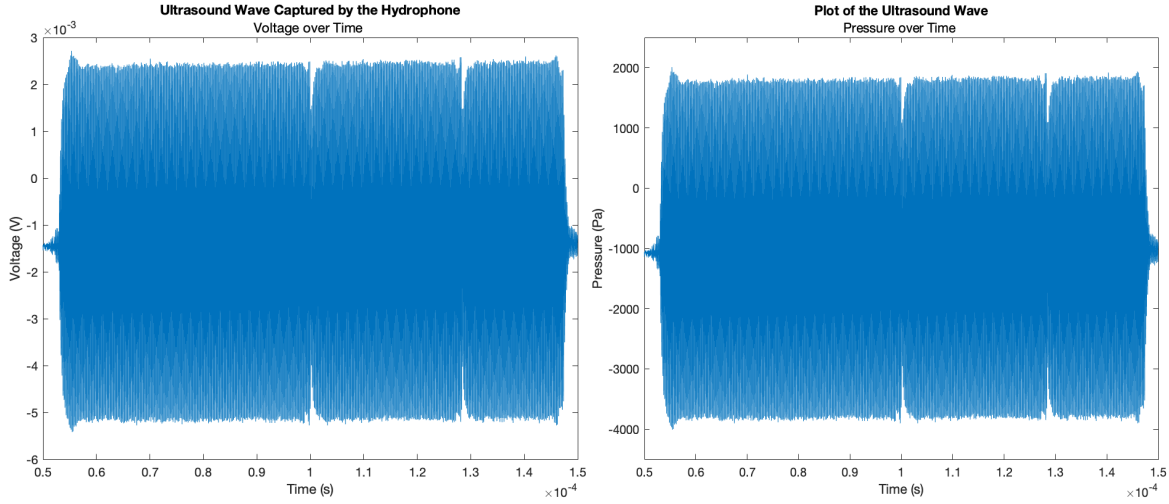

Figure 3.12 - *Ultrasound Wave sent by the HIFU transducer and captured by the hydrophone, after removing the electrical magnetic interference. On the left, there is a wave where two pulses have been removed, expressed in volts over time, and on the right, there is the same wave expressed in Mega Pascal over time.*

With the pressure over time wave, the envelope of the peaks of the points of the wave was done and the bottom part was removed since it was the mirror of the top part of the graph. The minimum value of the top part of the graph was added to all the values of the envelope in order to move the graph to zero. **Figure 3.13** represents the envelope of the ultrasound waves sent by the air-backing transducer. On the left, we have the envelope of the control wave and on the right, there is the envelope of the wave where two pulses have been removed. In **Figure 3.14** there is the envelope of the ultrasound waves sent by the HIFU transducer. On the left, we have the envelope of the control wave and on the right, there is the envelope of the wave where two pulses have been removed

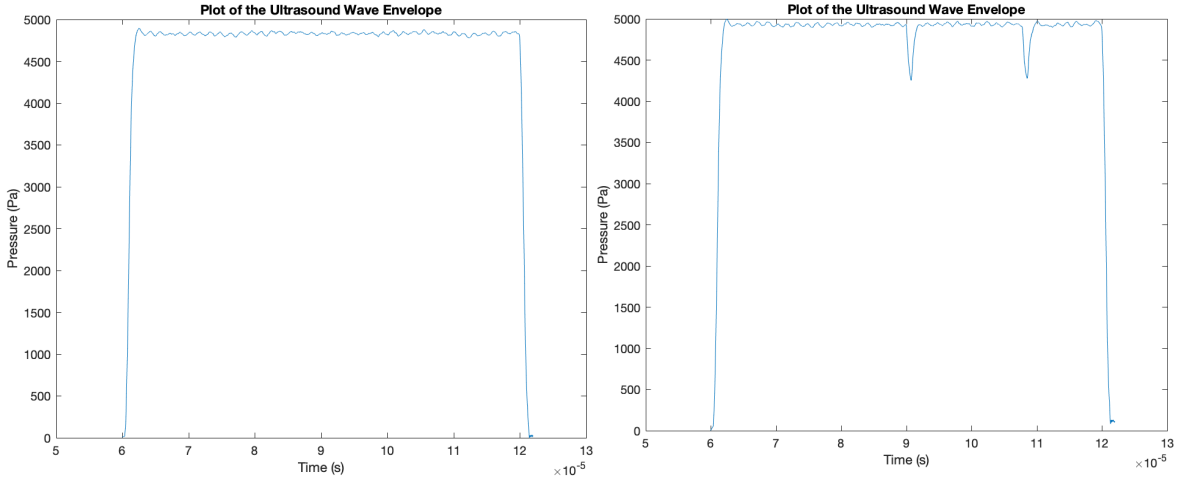

Figure 3.13 - *Ultrasound wave envelope in pressure over time of the wave generated by the air-backing transducer. On the left there is the envelope of the control wave and on the right, there is the envelope of the wave where 2 pulses have been removed.*

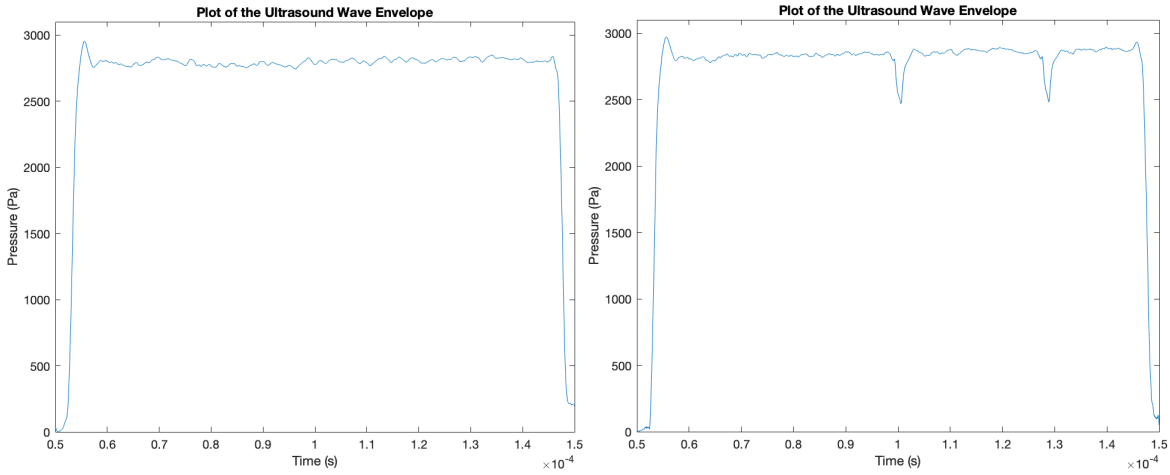

Figure 3.14 - *Ultrasound wave envelope in pressure over time of the wave generated by the HIFU transducer. On the left, there is the envelope of the control wave and on the right, there is the envelope of the wave where 2 pulses have been removed.*

All the values of our envelope were summed, and with that it was possible to calculate the average pressure, dividing the sum by the length of our data (number of points). The intensity was then calculated, **equation 3.1**, by dividing the square of the average pressure by two times the acoustic impedance of the ultrasound propagating medium (deionized water):

$$I = \frac{P^2}{2 \times Z} \tag{3.1}$$

As soon as we had all the envelopes, the data was normalized. The normalization was done by dividing the envelope values by their maximum value. The envelope of both the control wave and the envelope waveform with removed waves, are shown in **Figure 3.15** and **Figure 3.16**. All the values normalized on the envelopes were summed to calculate the area of the envelope and then divided by the length of the data to get an average value. This value was used as a metric for the intensity in order to compare in pairs the envelopes. To measure the percentage of loss, the average value of the envelope where some waves have been removed was subtracted from the average value of the control wave and then it was divided by the average value of the control wave multiplied by one hundred.

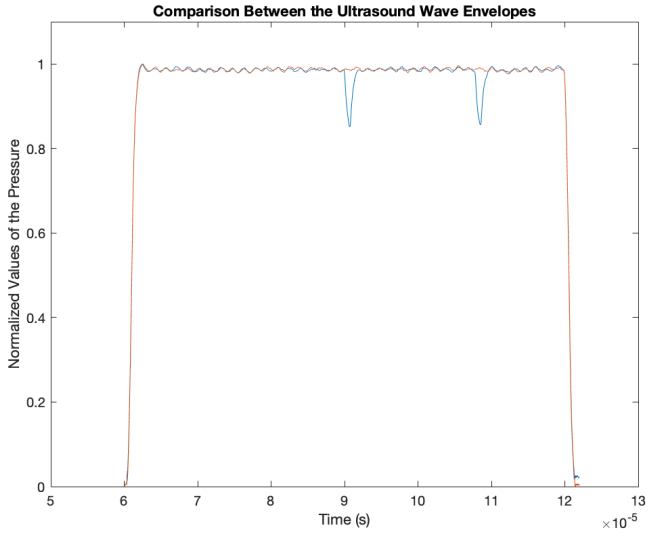

Figure 3.15 - *Overlapping envelopes of the waves generated by the Air-Backing transducer; Red: control wave; Blue: Wave without two pulses.*

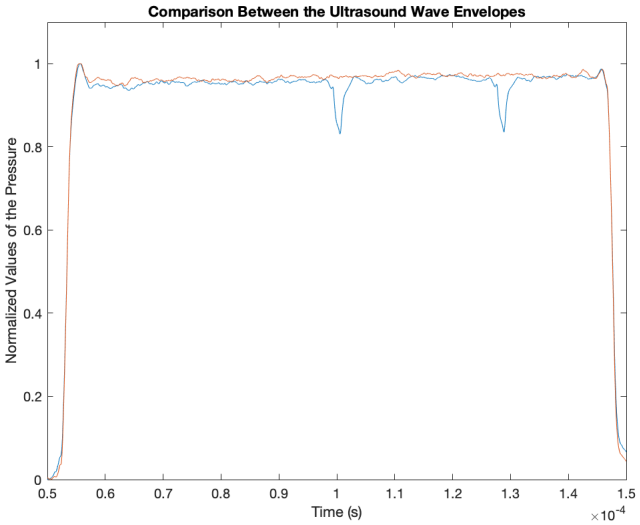

Figure 3.16 - *Overlapping envelopes of the waves generated by the HIFU transducer; Red: control wave; Blue: Wave without two pulses.*

3.3 EXPERIMENTAL SETUP OPEN CIRCUIT

In the previous experiment, each time a wave was removed from the waveform, we forced the short-circuit of two terminals across the PZT transducer to zero Volts. Instead of a short circuit, the goal was to have an open circuit whenever we wish to remove a wave in order to investigate if the short circuit was dampening the natural vibration of the PZT transducer and affecting the output intensity. Therefore, to achieve an open circuit, as desired, a circuit was projected and a Printed Circuit Board (PCB) was designed.

3.3.1 PCB Design

The PCB was designed using ALTIUM software (ALTIUM Designer Version 22.6.1, Release June 2022; Altium Limited, California, USA). First, a MOSFET (Metal Oxide Semiconductor Field Effect Transistor) driver (MD1213K6-G) was placed on the board. A MOSFET is used to control how much electricity can flow between the source and drain terminals depending on the amount of voltage applied to the gate terminal, and a MOSFET driver is used to drive the gate of the MOSFET efficiently in high-speed switching applications. To the output low supply voltage of the MOSFET driver, VL, we connect a capacitor of 1 μF to the ground. This capacitor is used as a stabilizer to counteract variations that can occur in the supplied voltage. The output high supply voltage 1 and 2 of the MOSFET driver, VDD1 and VDD2, were connected to a capacitor of 0.47 μF to 5 V voltage and to the ground. This capacitor is mitigating the noise at the power supply. Finally, the two output drivers, OUTA and OUTB, were linked to 2 capacitors of 10 nF each connected to the Gate of the N-channel and the gate of the P-Channel of the MOSFET (TC6320) to cancel the DC level from the signal. Two capacitors of 1 μF were placed on the PCB to be linked at the Source of the N-channel and the other one to the Source of the P-channel of the MOSFET in order to mitigate the noise. Connected to the Drain of the N-Channel and the Drain of the P-channel were 2 diodes in different directions. Those Diodes are used to allow current to flow in only one direction, they behave as a one-way switch for current. All the connections are shown in **Figure 3.17**.

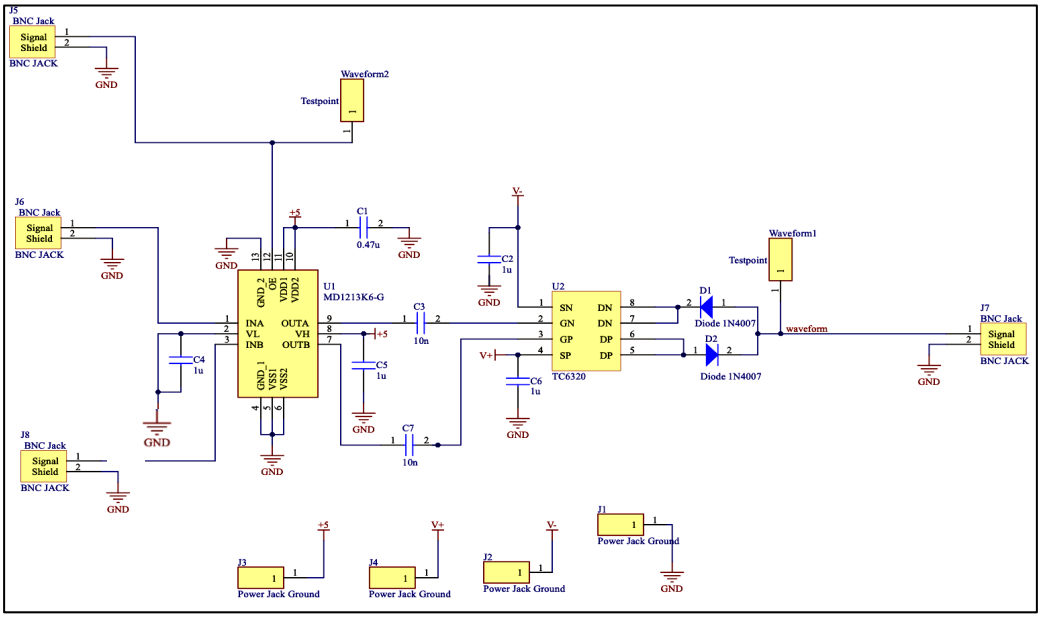

Figure 3.17 - *Image of the Printed Circuit Board Design: all the connections between the MOSFET and the de MOSFET Driver are described.*

In **Figure 3.18**, it is possible to observe the PCB already printed and soldered with the components described in the figure above. The transducer and the signal generator were connected to the PCB. Thus, the signal generator sent the wave created in MATLAB to the PCB and, the wave was then redirected to the transducer.

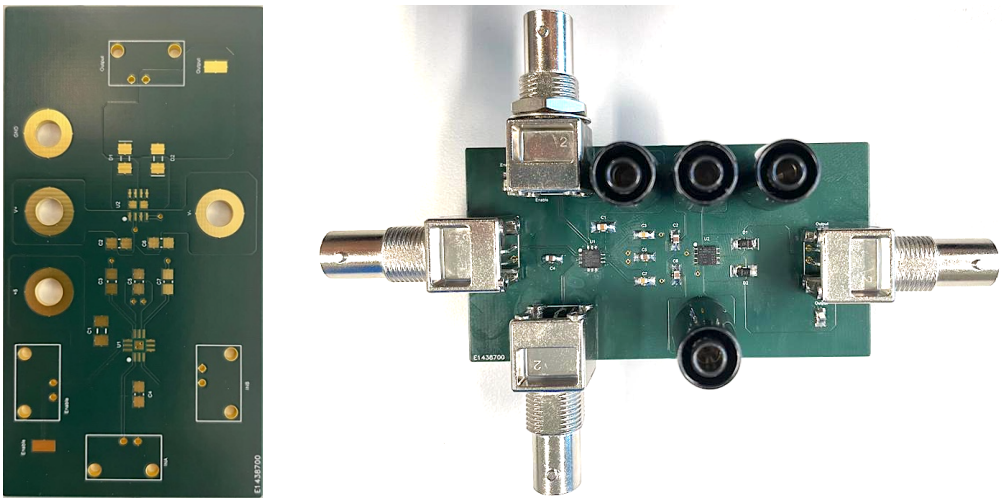

Figure 3.18 - *On the left there is the Printed PCB, and, on the right, there is the PCB with the components already soldered.*

As said before, the goal was to have an open circuit instead of a short circuit. Thus, we could not force the PZT to zero every time we would like to remove a pulse out of a complete waveform. Therefore, another MATLAB code was generated. A digital enable signal ranging from 0 (low) – 5 V (high) was created. Then to simulate the pulse removal, an output enable signal was built. This wave was programmed to be '1' whenever it was desired to measure the enable signal; otherwise, it would be '0', thus creating a measurement range. To remove a wave out of the waveform, the output enable signal was set to '0' inside the interval of '1', so it would be possible to send the signal to the other channel of the MOSFET, simulating a switch, **Figure 3.19**. After some nanoseconds, the output enable wave went back to '1', and the signal was sent again to the other channel of the MOSFET.

Figure 3.19 - *On the left, the green wave represents the enable signal ranging from 0 (low) – 5 V (high) and the yellow wave represents the output enable signal, where it is possible to identify two complete intervals where the measuring wasn't being done (0 V) and a complete interval of 5 V (measuring range interval) where one pulse had been removed (0 V inside of the measuring range interval); On the right, the green wave represents the output enable signal and the yellow wave was the signal that came from the PCB. It is also possible to see that the interval of removing a wave matched with a complete pulse of the yellow wave.*

In **Figure 3.20**, the wave that came from the PCB directly to the oscilloscope is shown. As we can see, the wave takes some time to reach its maximum value, the resonance frequency. Because of what s said previously, the number of pulses was set to 207 since it was the maximum number possible because of the dimensions of the water tank. Due to the increasing number of pulses, the transducer needed to be moved backward and, that is the reason for the decreasing values of voltage/pressure.

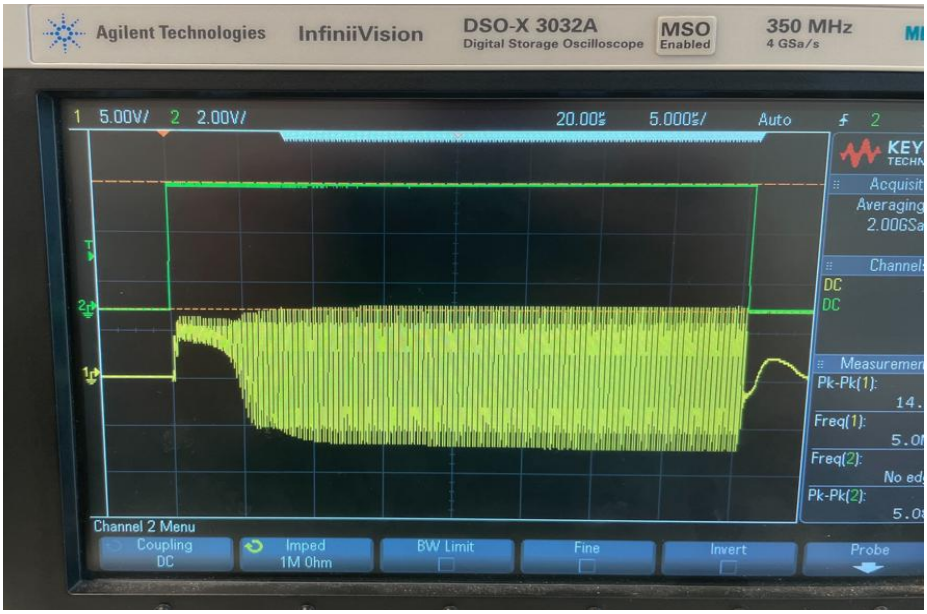

Figure 3.20 - *Wave that came from the Printed Circuit Board with 207 pulses.*

All the data that came from the oscilloscope was analyzed in the same way as the short circuit data. First, the voltage over time wave was plotted; Then the voltage was converted into pressure, and the pressure over time wave was also plotted. In **Figure 3.21** on the left, it is possible to see one example of an acquired control wave made with the PCB expressed in volts over time, and on the right, it is possible to see the same control wave expressed by pressure over time.

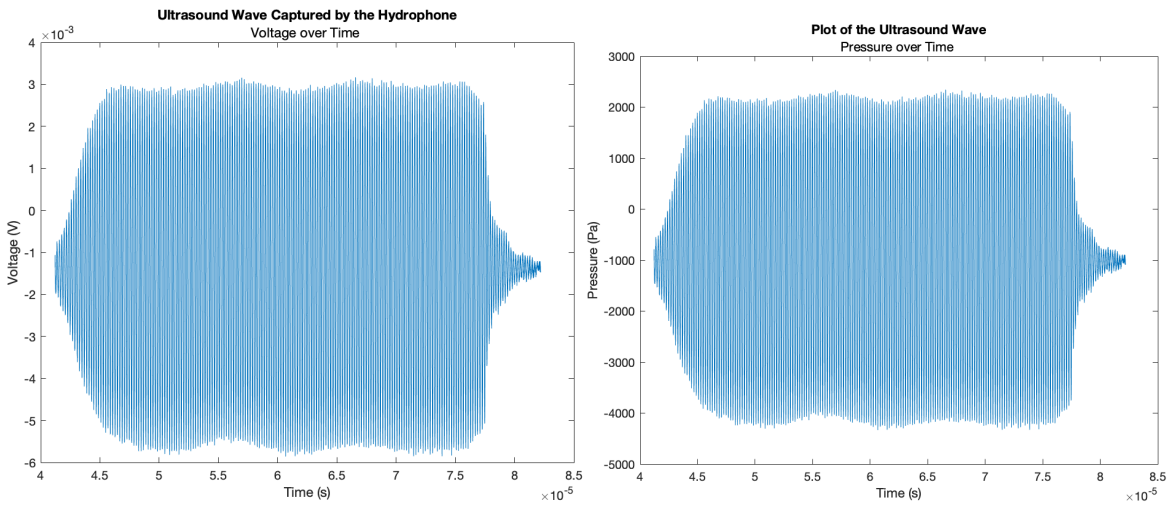

Figure 3.21 - *Ultrasound Wave that PCB sent to the transducer and captured by the hydrophone, after removing the electrical magnetic interference. On the left, there is a wave where two pulses have been removed, expressed in volts over time, and on the right, there is the same wave expressed in Mega Pascal over time.*

Figure 3.22 represents the plots of the waveforms where seven waves have been removed. On the left, the wave is expressed in volts over time and on the right, the wave represents pressure over time.

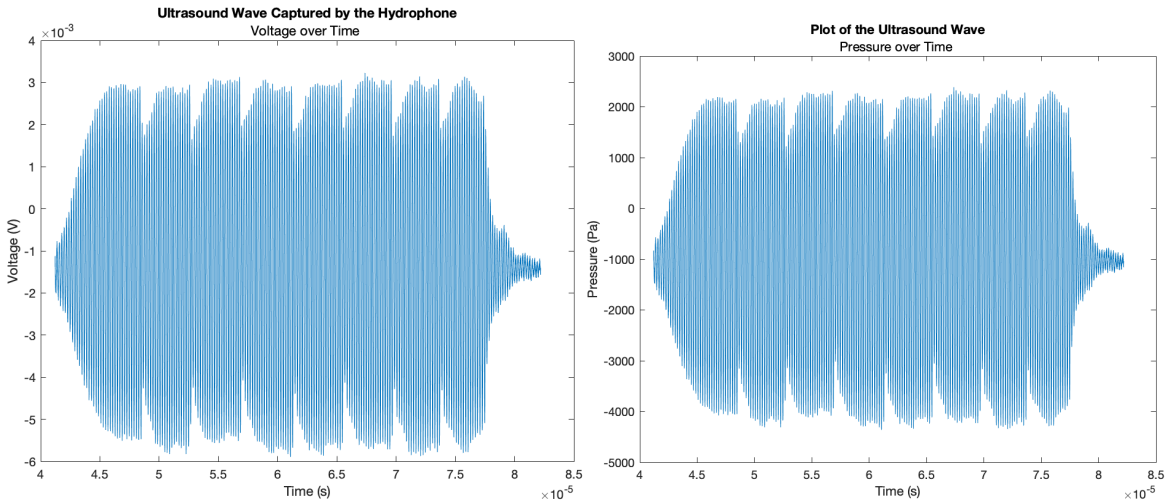

Figure 3.22 - *Ultrasound Wave that PCB sent to the transducer and captured by the hydrophone, after removing the electrical magnetic interference. On the left, there is a wave where seven pulses have been removed, expressed in volts over time, and on the right, there is the same wave expressed in Mega Pascal over time.*

Figure 3.23 represents the envelope of the ultrasound waves wave that PCB sent to the transducer. On the left, we have the envelope of the control wave and on the right, there is the envelope of the wave where seven pulses have been removed.

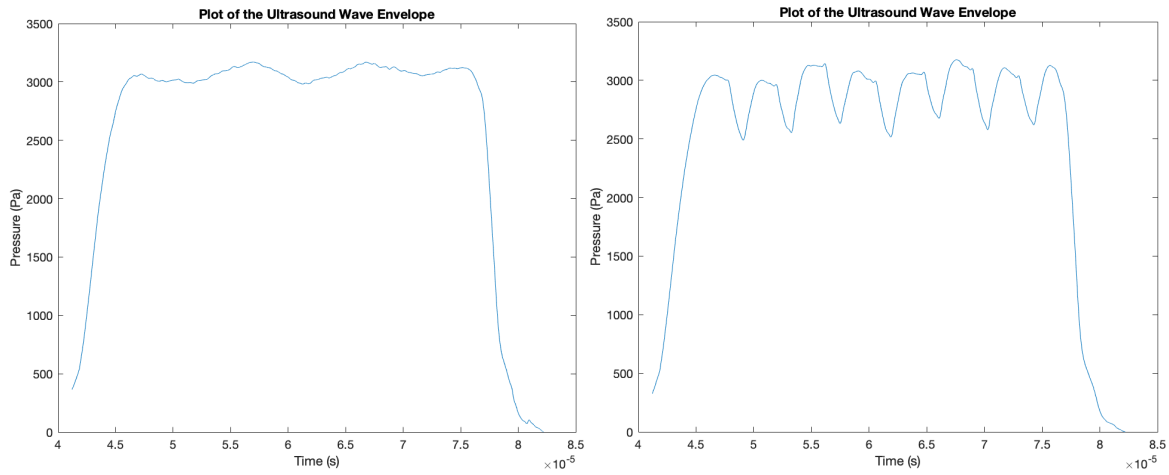

Figure 3.23 - *Ultrasound wave envelope in pressure over time of the wave that PCB sent to the transducer. On the left, there is the envelope of the control wave and on the right, there is the envelope of the wave where seven pulses have been removed.*

The envelope of each control wave was then plotted over the envelope of where waves have been removed, as we can see in **Figure 3.24**.

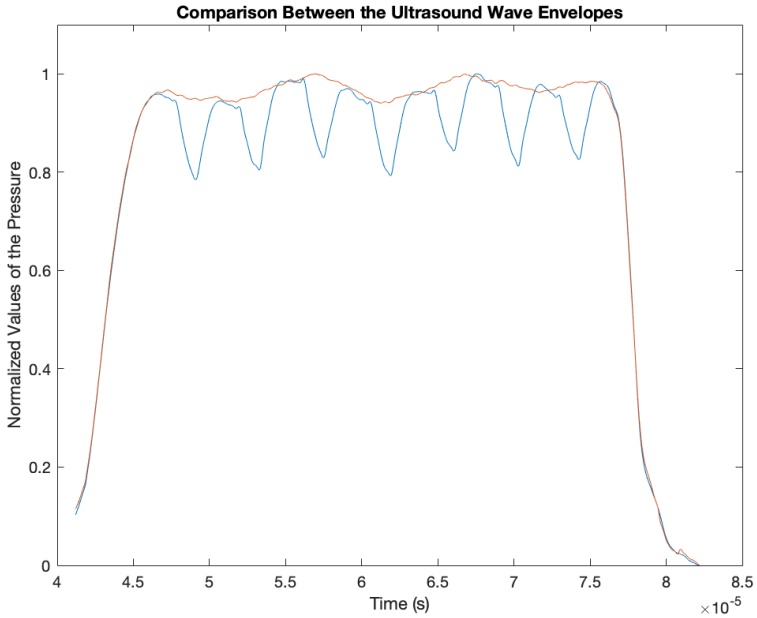

Figure 3.24 - *Overlapping envelopes of the waves generated transducer and sent by the PCB; Red: control wave; Blue: Wave without seven pulses.*

In conclusion, the setup used consisted of various electronics described above. Their operation was quite intuitive. In short, first, a signal was created with MATLAB software that was sent to the signal generator which returned it to the transducer; the hydrophone captured the signals from the transducer and sent them to the oscilloscope. The data was extracted from the oscilloscope to the computer and analyzed with a GUI, called EVA.

With this setup numerous measurements and experiments have been performed. In the following chapter, the results obtained from all the measurements described above will be demonstrated.

4 Results

This chapter aims to demonstrate the most pertinent results of this study. First, the results concerning the beam profile are presented, followed by the results of the acoustic wave removal simulation. Next, the data for the short circuit and open circuit are presented, and there is also a comparison between these two.

4.1 ULTRASOUND MATLAB CODE

4.1.1 Beam Profile

Using the k-wave toolbox from MATLAB it was possible to plot the beam profile of the three different planes in different circumstances. Firstly, the code did not take into consideration the waves being removed, **Figure 4.1** and **Figure 4.2**.

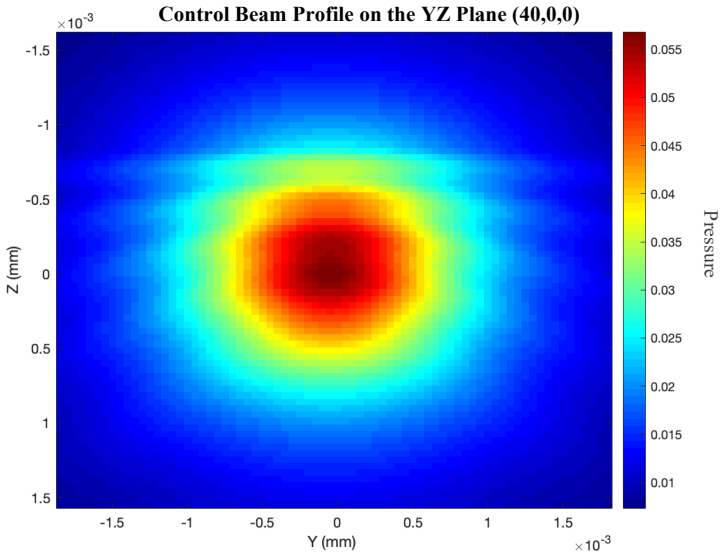

Figure 4.1- *Plot of the beam profile on the YZ plane without removing any wave (control wave).*

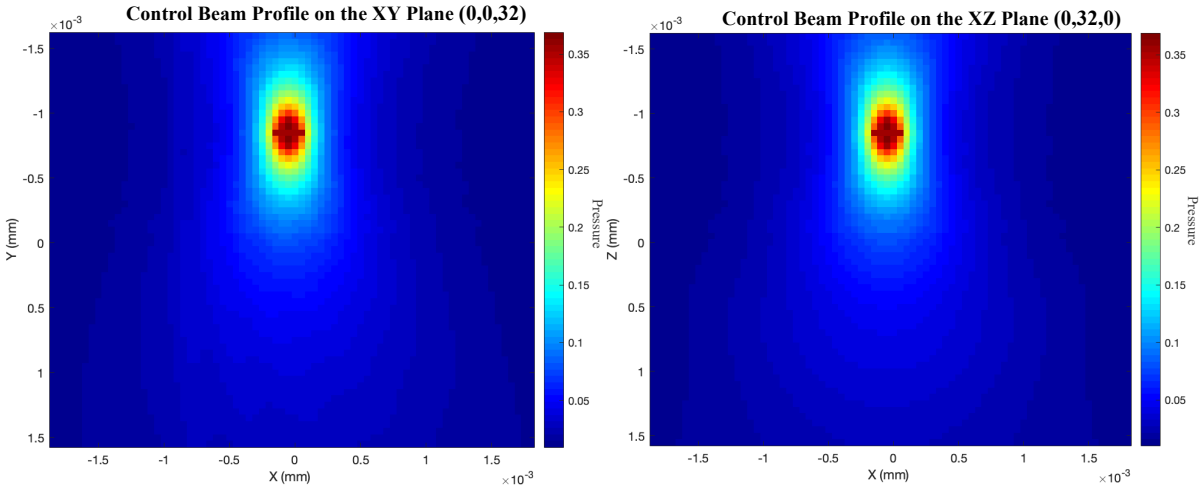

Figure 4.2 *- Plot of the beam profile without removing any waves (control wave). On the Left it is represented the beam profile on the XY plane and on the right the XZ plane.*

The control values for the maximum pressure value of the beam profile are around 0.056 u.p. (unitless pressure) for the YZ plane and around 0.37 u.p. for both XZ and XY planes. Through **Figure 4.2** it is perceptible that the beam profile from XY and XZ planes have the same values and shape.
After having the control waves for the 3 different planes, some waves had been removed to see their impact on the beam profile, **Figure 4.3 - Figure 4.6**.

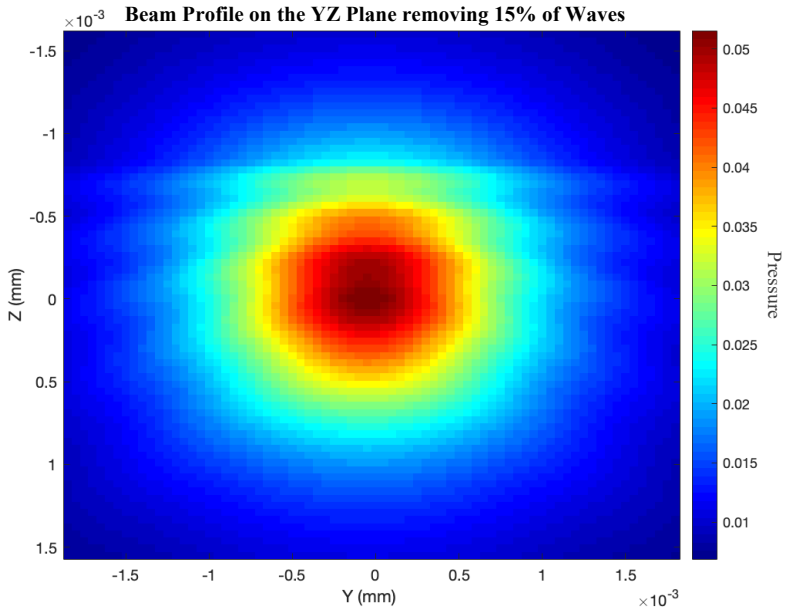

Figure 4.3 *- Plot of the beam profile on the YZ plane removing 15% of waves.*

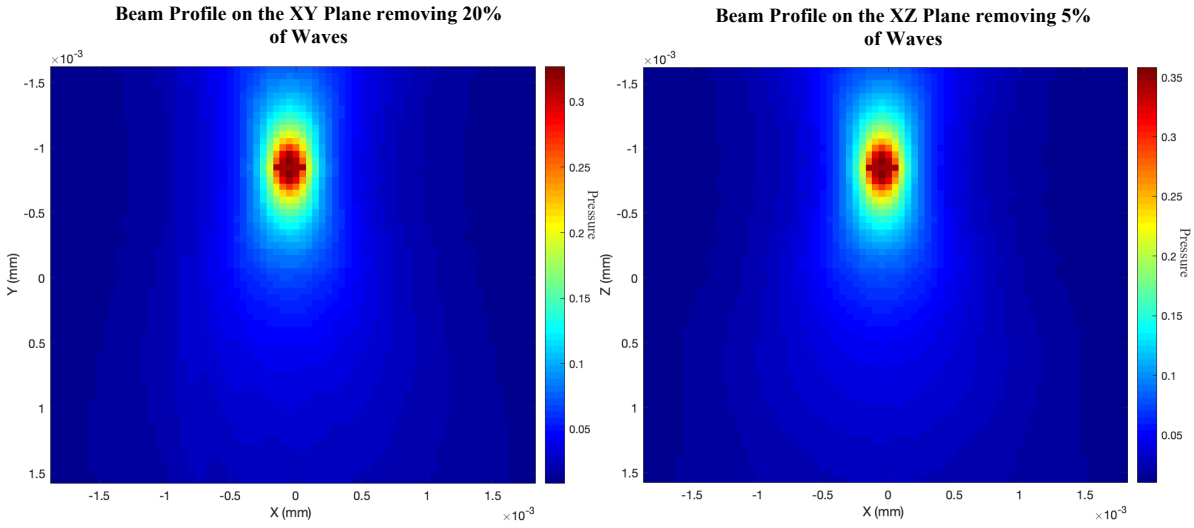

Figure 4.4 *- Plot of the beam profile removing some waves. On the Left it is represented the beam profile on the XY plane when it was removed 20% of waves from the waveform and on the right, it is represented the beam profile on the XZ plane when it was removed 5% of waves from the waveform.*

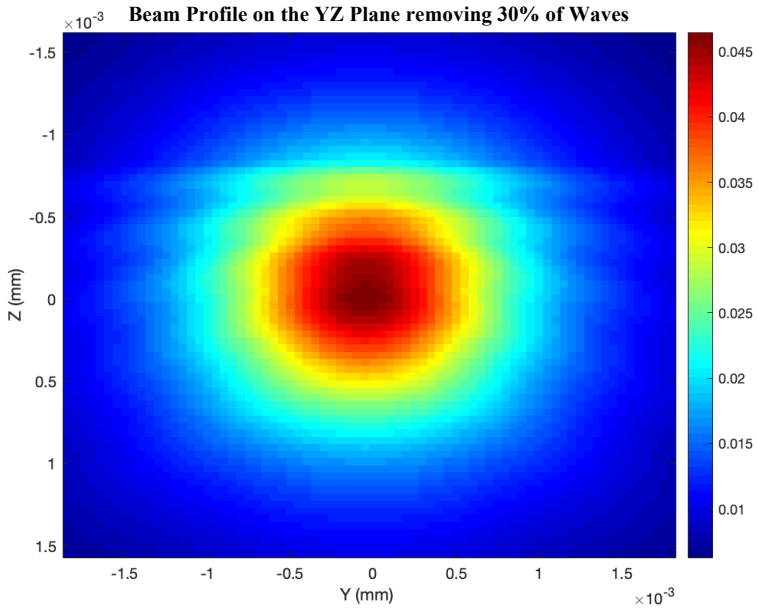

Figure 4.5 *- Plot of the beam profile on the YZ plane removing 30% of waves.*

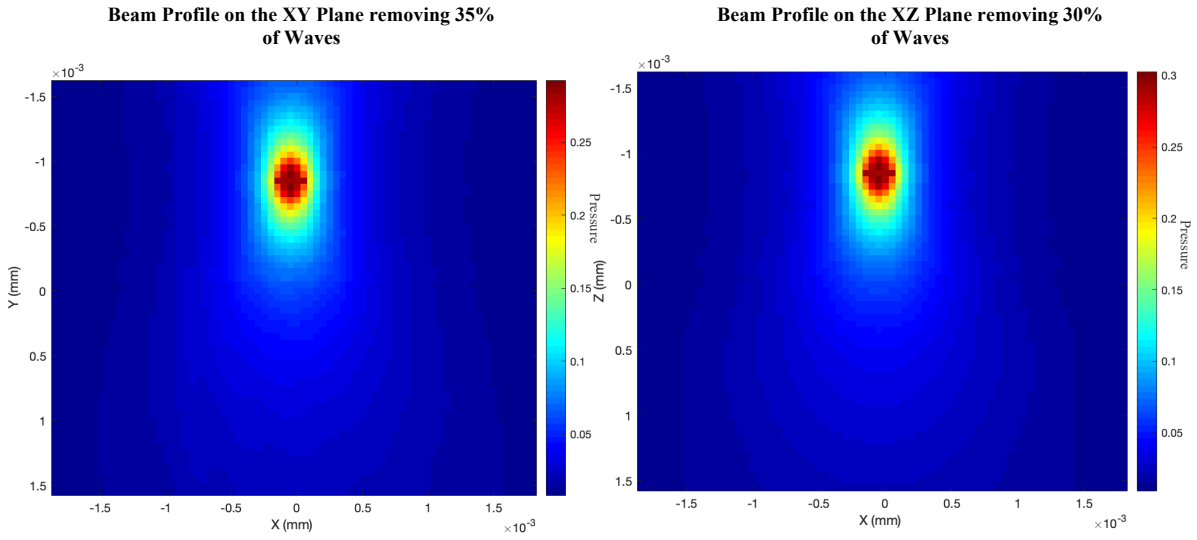

Figure 4.6 *- Plot of the beam profile removing some waves. On the Left it is represented the beam profile on the XY plane when it has been removed 35% of waves from the waveform and on the right, it is represented the beam profile on the XZ plane when it has been removed 30% of waves from the waveform.*

Visually comparing with the figures shown above it is noticeable that the shape of the beam profile has not changed.

Finally, bellow it is possible to see the beam profile, on the different three planes, where some random waves had less amplitude instead of being removed, **Figure 4.7 – Figure 4.9**.

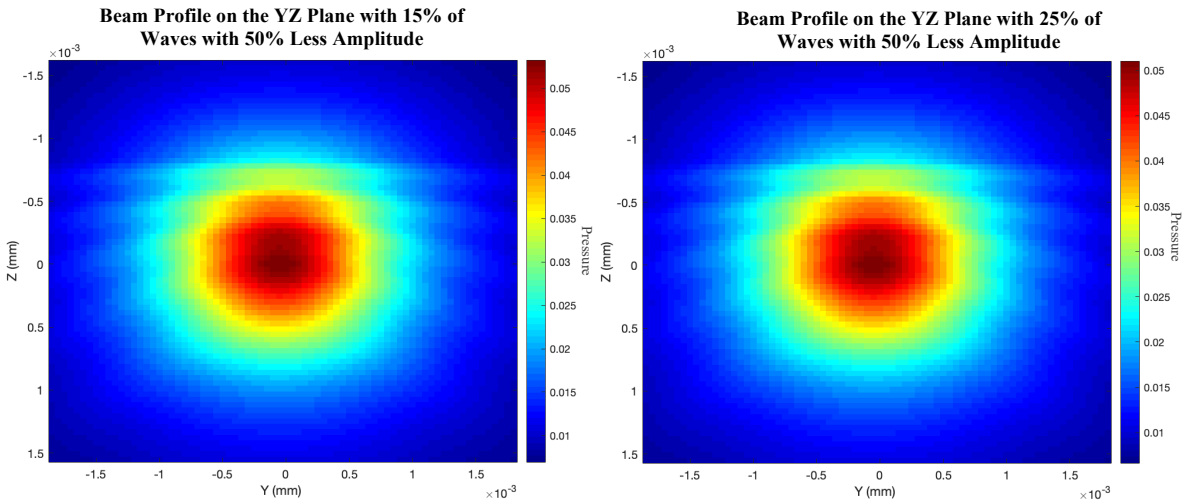

Figure 4.7 *- Plot of the beam profile where random number of waves have 50% less amplitude. On the Left it is represented the beam profile on the YZ plane when 15% of the waves from the waveform have 50% less amplitude and, on the right, it is represented the beam profile on the YZ plane when 25% of the waves have 50% less amplitude.*

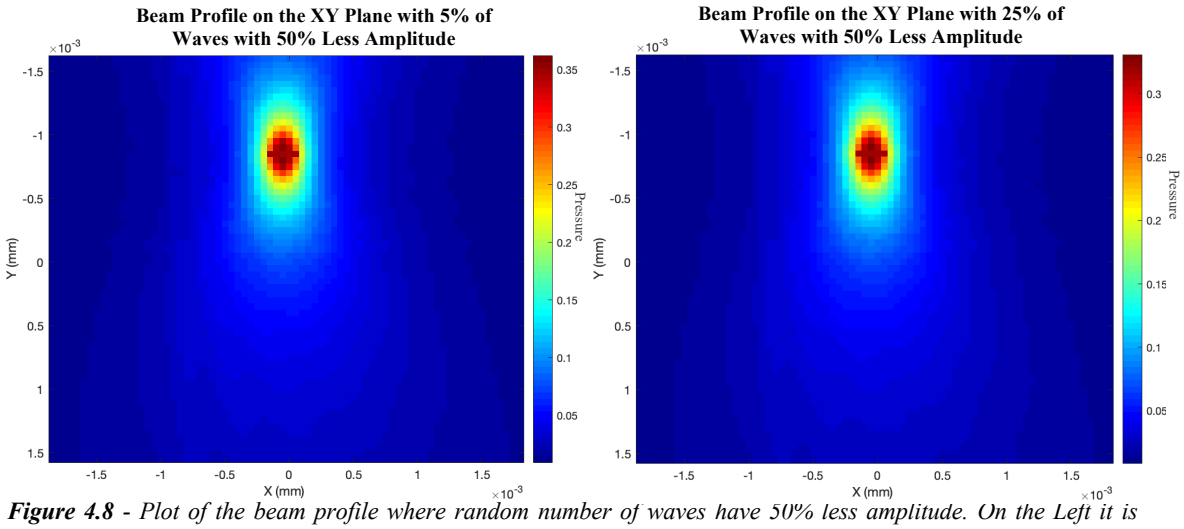

Figure 4.8 *- Plot of the beam profile where random number of waves have 50% less amplitude. On the Left it is represented the beam profile on the XY plane when 5% of the waves from the waveform have 50% less amplitude and, on the right, it is represented the beam profile on the XY plane when 25% of the waves have 50% less amplitude.*

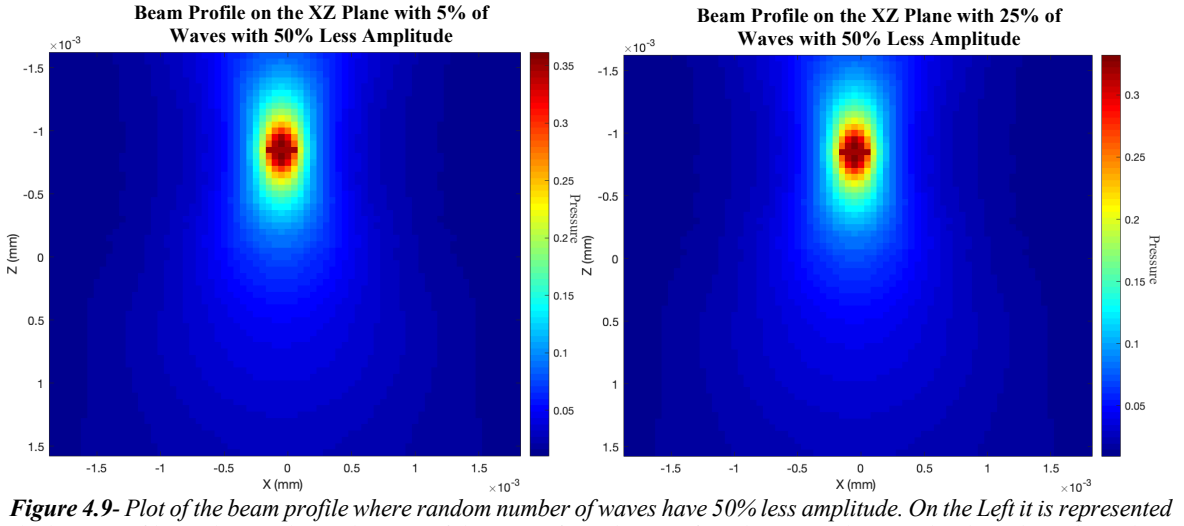

Figure 4.9*- Plot of the beam profile where random number of waves have 50% less amplitude. On the Left it is represented the beam profile on the XZ plane when 5% of the waves from the waveform have 50% less amplitude and, on the right, it is represented the beam profile on the XZ plane when 25% of the waves have 50% less amplitude.*

4.1.2. Acoustic Wave Removal Simulation

The maximum value of pressure while some waves have been removed was plotted. Since Planes XZ and XY have the same values, their results are plotted together.

In **Figure 4.10**, it is possible to realize that the maximum value of pressure when there are no waves being removed is around 0.37 MPa, and when 45% of waves are removed is around 0.18 MPa. Having these values, it is possible to calculate the decay from the first instant until pulses are removed. So, it decays by about 0.19 MPa when 45% of the pulses are removed.

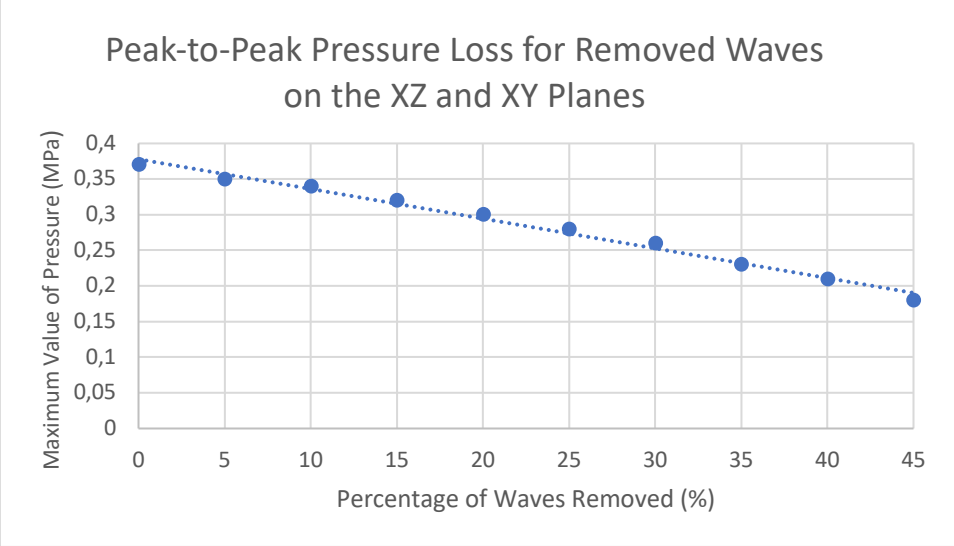

Figure 4.10 *– Plot of the peak-to-peak pressure variation with wave removal on the XZ and XY Planes.*

Figure 4.11 represents the plot of the peak-to-peak pressure for removed waves on the YZ plane. It is possible to see that the maximum value of pressure when there are no waves removed is around 0.056 MPa, and when 45% of waves are removed is around 0.027 MPa. Then, it decreases by 0.029 MPa when 45% of the pulses are removed.

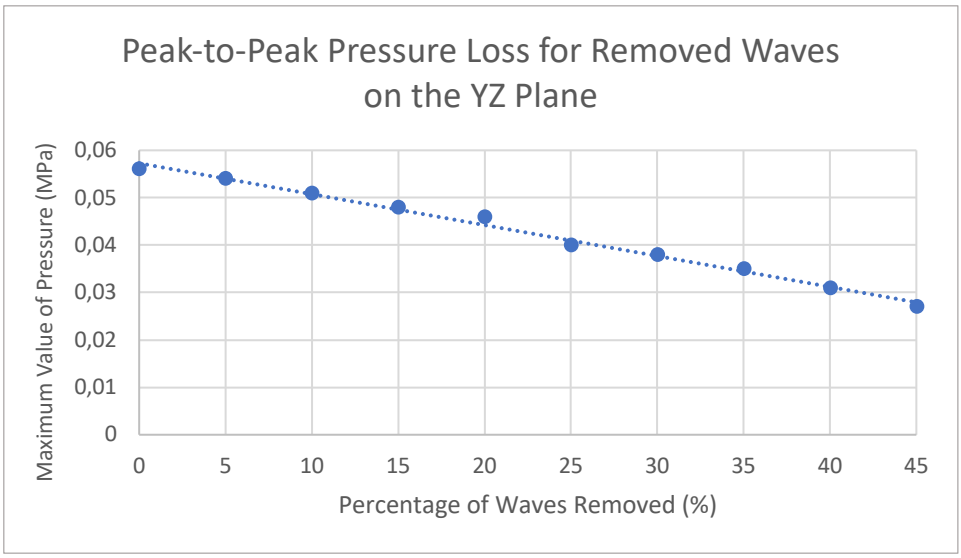

Figure 4.11 *- Plot of the peak-to-peak pressure variation with wave removal on the YZ Plane.*

Figure 4.12 is the representation of the plot of the peak-to-peak pressure for removed waves on the XZ and XY planes from a burst of pulses. It is possible to see that the maximum value of pressure when there are no waves being removed is around 0.37 MPa, and when 45% of waves are removed is around 0.20 MPa. Therefore, the decay is about 0.17 MPa.

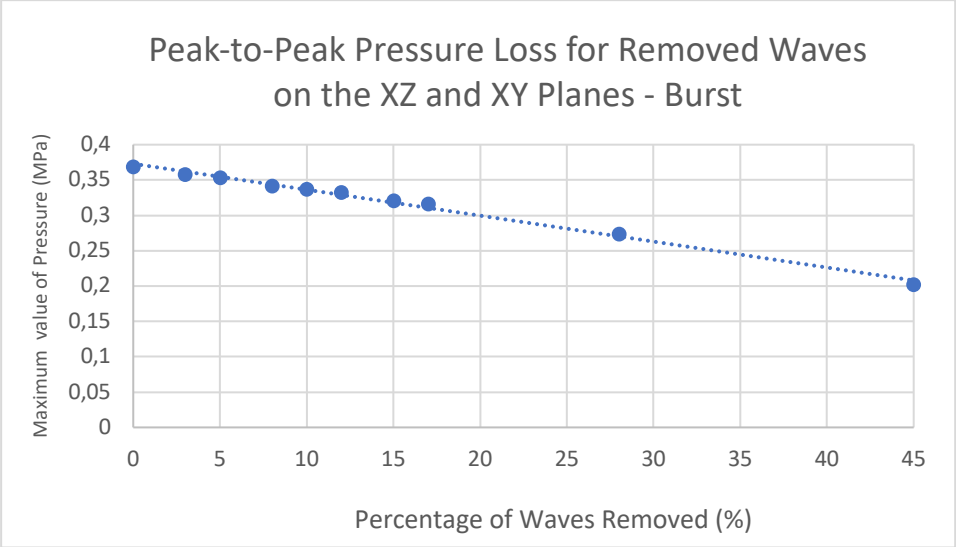

***Figure 4.12** - Plot of the peak-to-peak pressure variation with wave removal on the XZ and XY Planes for a burst of pulses.*

In **Figure 4.13**, there is the representation of the plot of the peak-to-peak pressure for removed waves on the YZ Plane from a burst of pulses. It is possible to see that the maximum value of pressure when there are no waves being removed is around 0.056 MPa, and when 45% of waves are removed is around 0.030 MPa, decreasing by 0.026 MPa.

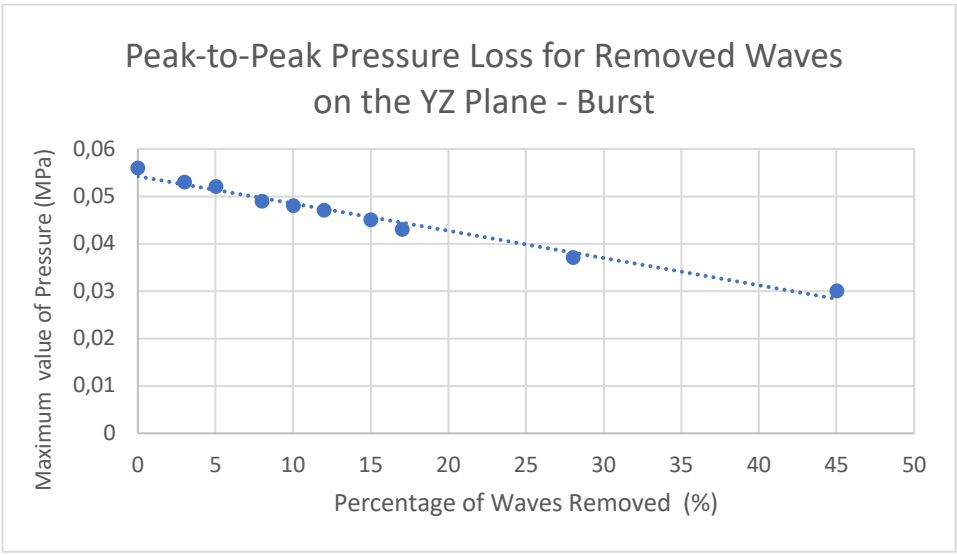

***Figure 4.13** - Plot of the peak-to-peak pressure variation with wave removal on the YZ Plans for a burst of pulses.*

In **Figure 4.14**, we can see the plot of the peak-to-peak pressure variation with the wave's amplitude reduced by 50% in the XZ and XY Planes. It is possible to see that the maximum value of pressure when there are no waves with less amplitude is around 0.37 MPa, and when 45% of the waves have 50% less amplitude is around 0.23 MPa. Subtracting the values, it can be concluded that the difference between 45% of the reduced pulses and no pulse reduced is 0.14 MPa.

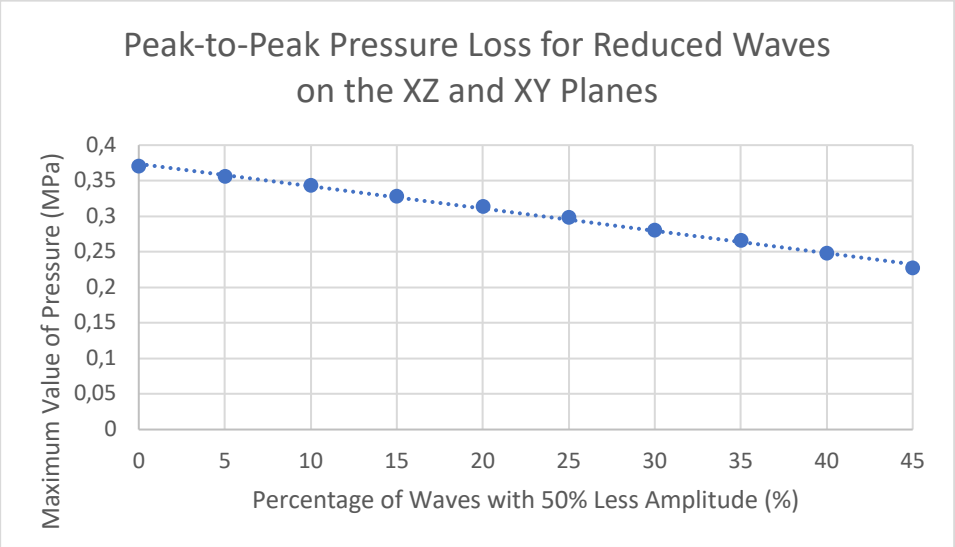

Figure 4.14 *- Plot of the peak-to-peak Pressure Variation with the Wave's Amplitude Reduced by 50% in the XZ and XY Planes*

In **Figure 4.15**, we can see the plot of the peak-to-peak pressure variation with the wave's amplitude reduced by 50% in the YZ Plane. It is possible to see that the maximum value of pressure when there are no waves with less amplitude is around 0.056 MPa, and when 45% of the waves have 50% less amplitude is around 0.034 MPa. So, it decreases by 0.022 MPa.

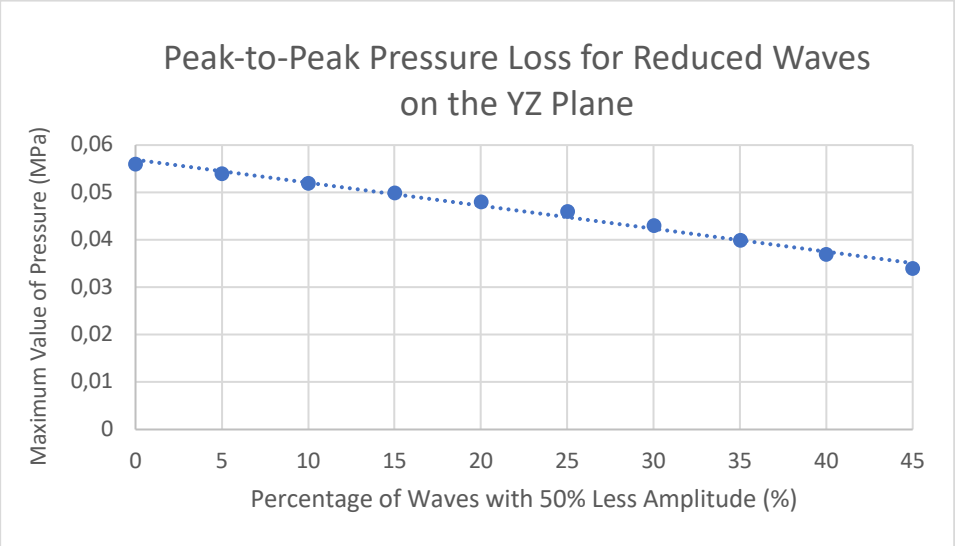

Figure 4.15 *- Plot of the peak-to-peak Pressure Variation with the Wave's Amplitude Reduced by 50% in the YZ Plane.*

In **Figure 4.16**, we can see the plot of the peak-to-peak pressure variation with the wave's amplitude reduced by 50% in the XZ and XY Planes from a burst of pulses. It is possible to see that the maximum value of pressure when there are no waves with less amplitude is around 0.37 MPa, and when 45% of the waves have 50% less amplitude is around 0.25 MPa. The decay is around 0.12 MPa.

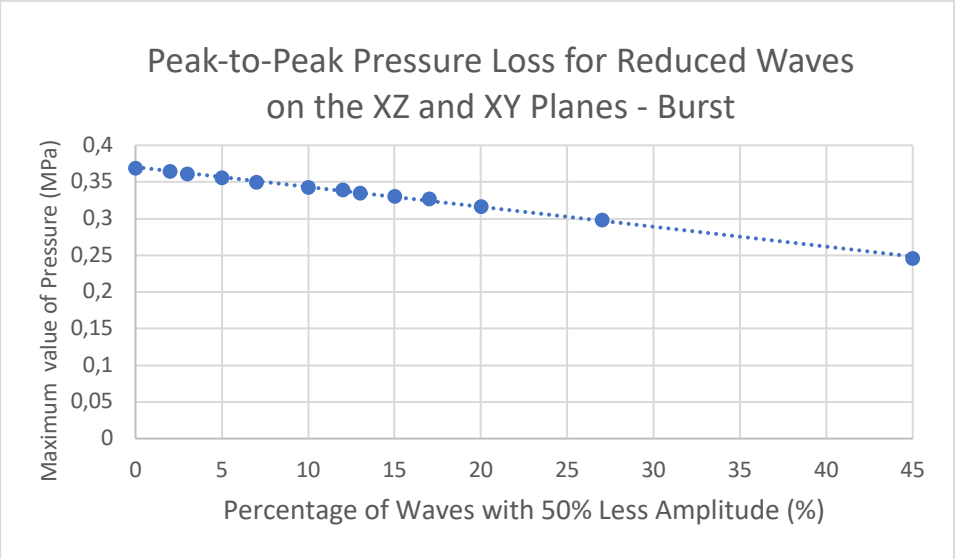

***Figure 4.16** - Plot of the peak-to-peak Pressure Variation with the Wave's Amplitude Reduced by 50% in the XZ and XY Planes from a burst of pulses.*

In **Figure 4.17**, we can see the plot of the peak-to-peak Pressure Variation with the Wave's Amplitude Reduced by 50% in the YZ Plane from a burst of pulses. It is possible to see that the maximum value of pressure when there are no waves with less amplitude is around 0.056 MPa, and when 45% of the waves have 50% less amplitude is around 0.038 MPa. In this experiment, the decay is around 0.018 MPa.

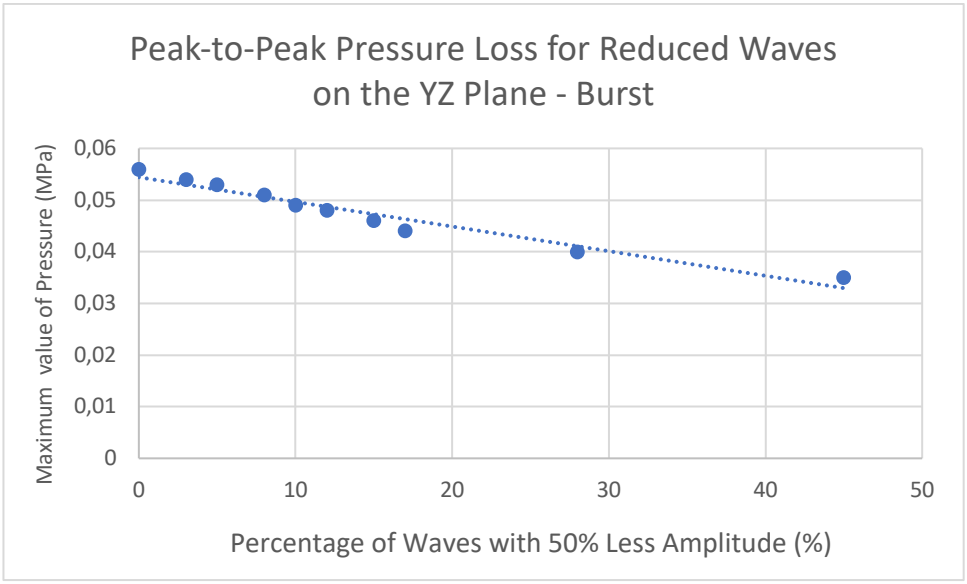

***Figure 4.17** - Plot of the peak-to-peak Pressure Variation with the Wave's Amplitude Reduced by 50% in the YZ Plane from a burst of pulses.*

Through the observation of all the images in this chapter, it can be noticed that as entire pulses are removed, the maximum pressure value decreases linearly. The same occurs when the number of waves with the pulse amplitude reduced by 50% increases. However, it should be noted that the pressure drop is smaller in the case where the waves have reduced amplitudes in a few pulses.

4.2 EXPERIMENTAL SETUP SHORT CIRCUIT

All the data from the two different transducers, the Air-backing transducer, and the HIFU transducer was taken. As said in the methods, the plot of the control waves and the waves that pulses have been removed were analyzed and compared. With all the data coming from the envelopes of the pressure over time waveforms it was possible to make the graph shown below. **Figure 4.18** represents the percentage of intensity loss of both air-backing and HIFU transducer.

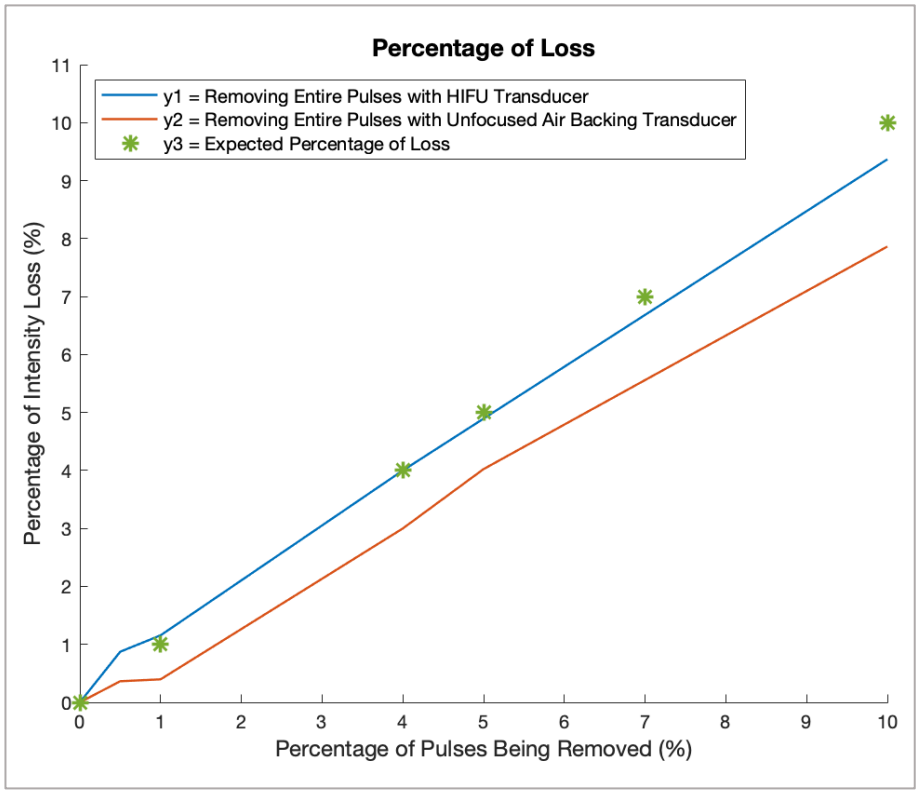

Figure 4.18 *– Comparison of percentage of loss of both Air-backing and HIFU transducers. The blue line represents the HIFU transducer, and the red line represents the air-backing transducer. The green asterisks represent the expected percentage of loss by removing the percentage of pulses shown.*

In **Figure 4.18**, the green asterisks represent the expected percentage of loss, which means, the energy that is expected to be lost, in percentage, without sending some pulses. It is considered the expected percentage of loss the energy of the pulses that are not being sent, i.e., if it is not sent 10% of pulses the expected loss is 10%. As it is possible to note, the blue line, the HIFU transducer, loses around 5% of energy when around 5% of pulses are removed from the waveform. On the other hand, the red line, the

air-backing transducer, loses around 3.5% of energy when the same number of pulses are removed as before.

Figure 4.19 shows the representation of the percentage of intensity loss of the air-backing transducer. As before, the green asterisks represent the expected percentage of loss or, in other words, the percentage of energy saved.

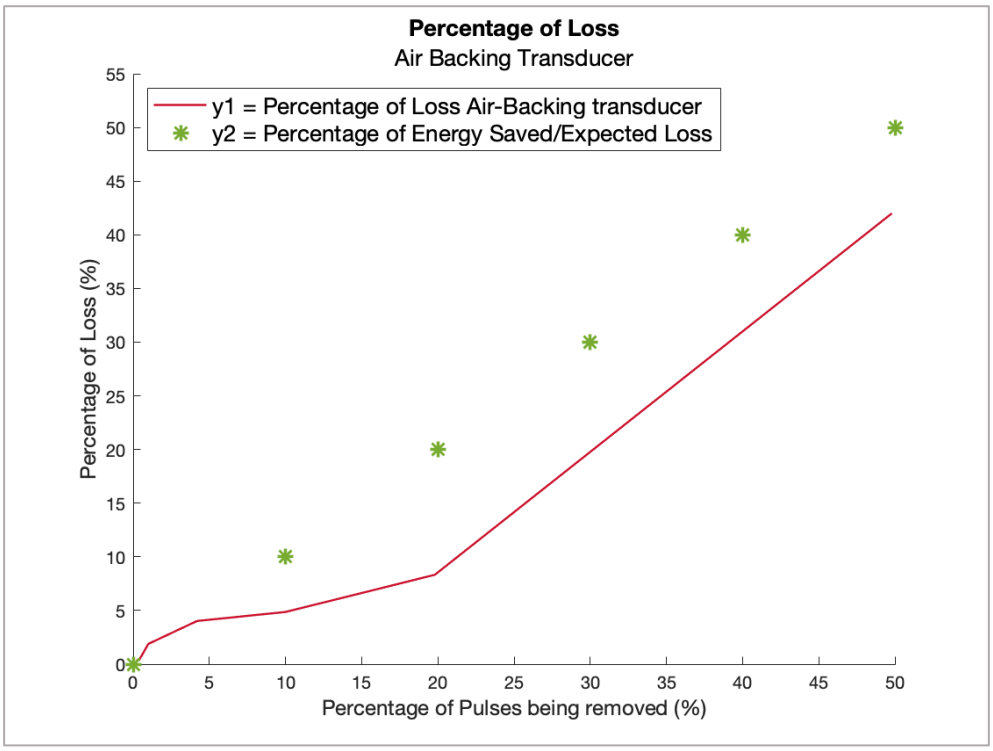

Figure 4.19 *- Percentage of loss of Air-backing transducer. The red line represents the percentage of loss when some pulses are being removed. The green asterisks represent the expected percentage of loss by removing the percentage of pulses shown, which corresponds to the percentage of energy saved.*

Through **Figure 4.19**, it is possible to see that the red line is always below the green asterisks, and, for example, when it is saved around 30% of energy, the percentage of loss is around 20%.

Figure 4.20 illustrates the difference in the percentage of loss when entire pulses are removed out of the waveform or only a part of them. The blue line represents the percentage of loss removing entire pulses, the red line represents the percentage of loss removing 50% of the amplitude of the pulses and the yellow line represents the percentage of loss removing only 30% of the amplitude of the pulses.

As it is possible to see in the graph, when entire pulses are removed, blue line, around 42% of energy is lost when it is removed from the waveform around 50% of pulses. On the other hand, when it is removed only 50% of the amplitude of 50% of the pulses, red line, around 15% of energy is lost. Finally, when it is removed only 30% of the amplitude of 50% of the pulses, the yellow line, around 4% of energy is lost.

Through these results, it is observed that the energy saved by not being sent is higher than the energy lost, thus it is verified that it is indeed possible to save energy through this method, and these results are once again in agreement with the hypothesis under study.

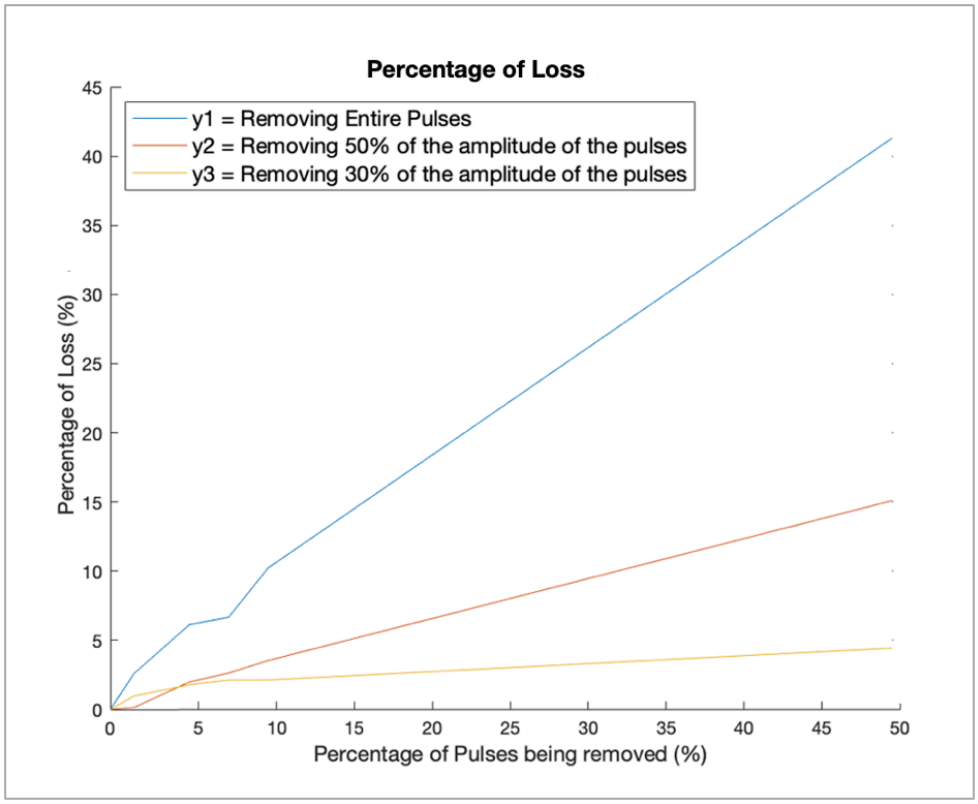

Figure 4.20 *– Comparison of Percentage of loss between removing entire pulses out of the waveform and removing only a part of the amplitude of a few pulses. The blue line represents the percentage of loss removing entire pulses, the red line represents the percentage of loss removing 50% of the amplitude of the pulses and the yellow line represents the percentage of loss removing only 30% of the amplitude of the pulses.*

4.3 EXPERIMENTAL SETUP OPEN CIRCUIT

After having all the data and results from the short circuit, the next step was evaluating the data from the open circuit, in other words, the data was prevenient from the measurements using the PCB as a switch.

Figure 4.21 representes the plot of the percentage of loss where some pulses were being removed from the waveform. As we can see in the figure, when around 10% of the pulses are removed from the waveform, the percentage of loss is around 15%.

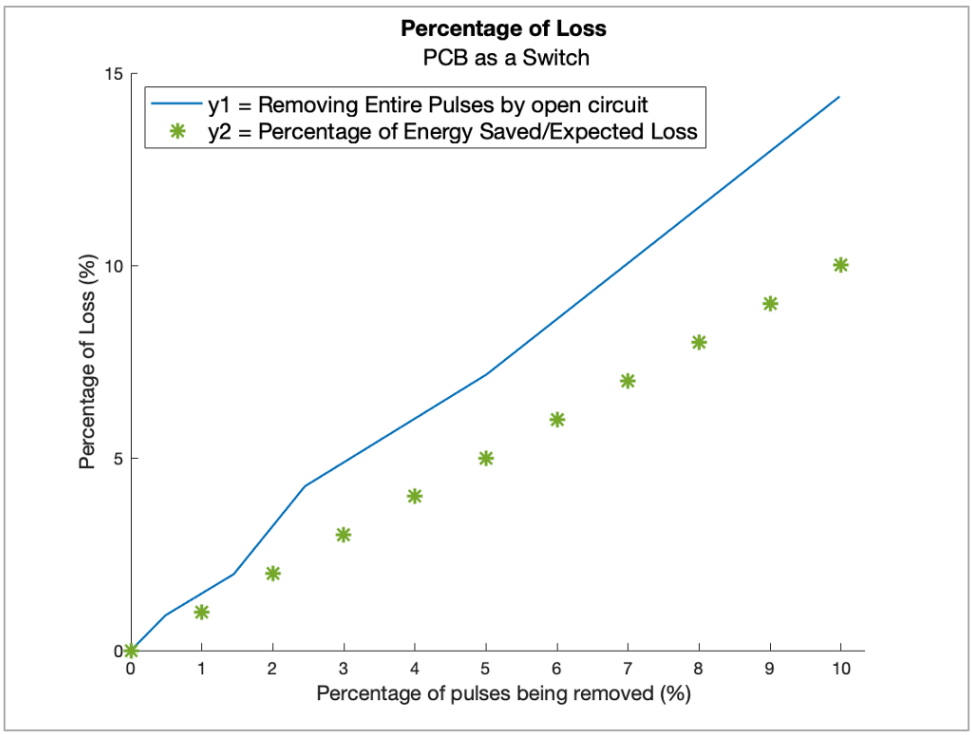

Figure 4.21 *- Percentage of loss using the PCB. The blue line represents the percentage of loss when some pulses are being removed. The green asterisks represent the expected percentage of loss by removing the percentage of pulses shown, which corresponds to the percentage of energy saved.*

4.4 SHORT CIRCUIT VS OPEN CIRCUIT

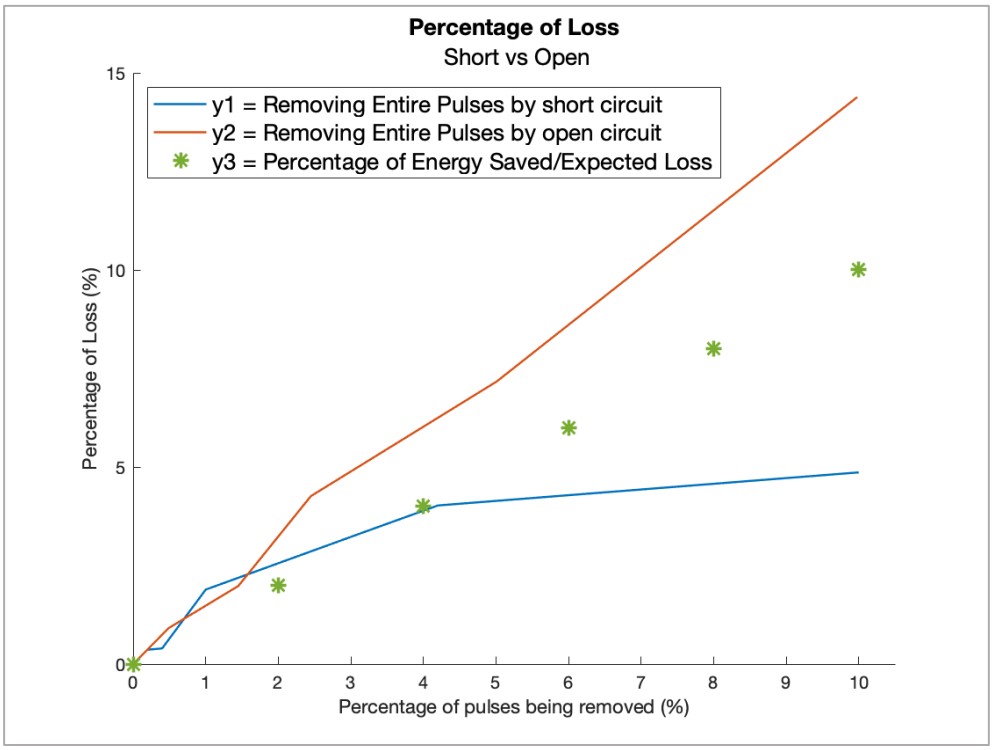

Figure 4.22 *- Comparison of Percentage of loss between short and open circuits. The blue line represents the percentage of loss removing entire pulses by short circuit and, the red line represents the percentage of loss removing pulses by an open circuit. The green asterisks represent the expected percentage of loss by removing the percentage of pulses shown, which corresponds to the percentage of energy saved.*

In **Figure 4.22**, we have a comparison of the percentage of loss between short and open circuits. As before, the green asterisks represent the expected percentage of loss or, in other words, the percentage of energy saved.

In the graph, it is possible to see that the percentage of loss from the open circuit (red line) is much higher than the percentage of loss from the short circuit (blue line). It is also possible to conclude that the open circuit has always higher values than the asterisks and in the other hand the short circuit has most of the time lower values of percentage of loss than the values of the green asterisks.

5 Discussion

This chapter will provide a brief overview of the limitations in the measurements acquired and possible errors will then be discussed. Firstly, the observed results of the beam profile are discussed here as well as those of the acoustic wave removal simulation. Then, a brief discussion of the results of the short circuit with the two different transducers as well as the open circuit is given. Lastly, a comparison between the latter two will be performed in order to understand which one showed better results and a possible explanation for this.

5.1 ULTRASOUND MATLAB CODE

5.1.1 Beam Profile

The ultrasound beam profile simulation provides the calculated transmitted ultrasound pressure field for a given transducer aperture at a particular plane transverse to the beam propagation path. The study's first goal was to understand the behavior of the beam profile in different situations, such as removing complete pulses or just reducing their amplitude.

Through the images related to the simulations of the beam profile, **Figure 4.1** to **Figure 4.9**, it is shown that the beam profile shape never changes, and the maximum pressure value only registered small changes. In theory, it is expected that the maximum value of the pressure will decrease as pulses are removed from the complete waveform since there are some deflections in the wave each time a pulse is removed. These deflections cause a decrease in the voltage and subsequently in the pressure value. However, as seen in the figures, the maximum pressure value shown in the beam profile only suffers small differences. Since there are just some of the pulses being removed, it is possible that the program took a sample from somewhere else in the waveform to form the beam profile instead of the sample where the pulse was removed from.

The shape of the beam profile changes with the beam pressure. Since the pressure of the beam barely changes, the shape remains constant. It is also possible to see that when only a part of the amplitude of the pulse is removed, instead of the complete pulse, the maximum pressure value decreases less than when we remove the complete pulse from the waveform, as expected.

5.1.2 Acoustic Wave Removal Simulation

The second goal of this project was to understand if the pressure value of the ultrasonic beam decreased as pulses were removed, and how the wave behaved with those decays. It was expected to decrease linearly since the only difference observed on the oscilloscope between removing one or two pulses is the number of depths, e.g, two depths are registered when two pulses are removed and only one depth is seen when one pulse is removed. The same behavior is visualized regardless of how many pulses are removed from the waveform.

In the plot of the peak-to-peak pressure for removed waves on the XZ and YZ planes, **Figure 4.10**, it is possible to observe that the maximum pressure value is always decreasing in a linear way as pulses are removed. The same linear behavior is seen in the plot of the peak-to-peak pressure for removed waves in the YZ plane, **Figure 4.11**. The values from the YZ plane are always smaller than the values from the XZ and XY planes since the YZ plane is not exactly in the middle of the focal spot.

Afterward, there are represented the same peak-to-peak pressure for removed waves graphs but this time considering that it is a set of pulses - burst. The initial values of both plots are the same as previously shown since we have not removed any pulse, regardless of whether it is a single waveform or a burst of waveforms. So, the hydrophone is always going to capture the first pulse and send it to the oscilloscope. The first pulse is going to have an equal value in every simulation. In both cases, the maximum pressure value when 45% of the pulses are removed is higher than before, and the decay is smaller. This may be due to the fact that in the latter cases, there is a burst of waves and therefore there may be more waves that can compensate for the loss, ending up being less noticeable in the maximum pressure value.

Thereafter, the pressure variation with the wave's amplitude reduced by 50% was plotted. Since there are no waves removed in the beginning, the initial value was again the same for all the planes, for the same reason as before.

Finally, the pressure variation with the wave's amplitude reduced by 50% in a burst was plotted. Thus, from the results presented above, it can be stated that the maximum value of the pressure is higher in the case where the wave's amplitude is reduced by 50% in a burst, and the decay is lower in this case as well.

From the acoustic wave removal simulation, it is possible to conclude that better results are obtained when reducing the wave amplitude by 50% in comparison to removing entire pulses from the waveform. It is worth mentioning that several errors are associated with these measurements, and therefore may have an influence on the results. First, the water tank in these simulations was installed on an unstable bench, as can be seen in **Figure 3.6**. Thus, it could tremble with a few simple steps of people, fiddling with the computer to save the results, with the wind each time the door was opened, or simply with human speech. Some of these factors were considered, attempting to minimize these errors as much as possible by not moving or talking during data acquisition. Another possible error is that the cables are long and intertwined in order to reach the respective connection point, adding impedance and resistance to the measurements.

5.2 EXPERIMENTAL SETUP SHORT CIRCUIT

The third goal of this thesis project was to find out under laboratory conditions whether it was possible to save some energy from the ultrasound by removing some pulses or decreasing their amplitude and discover which transducer would be better for saving energy. That is, for instance, if we remove ten percent of the pulses from the wave and lose any value less than ten percent of energy, we are saving some energy.

In the short circuit measurements, it should be noted that the water tank was already installed on the optical table, as it can be observed in **Figure 3.8**, which greatly reduced measurement errors associated

with vibrations from the surrounding space. The optical table was tested, and the measurements were no longer changed immediately by human steps or fiddling with the computer.

Those measurements were performed using the HIFU transducer and the unfocused air-backing transducer. **Figure 4.18** shows a comparison between them. As can be observed in the figure, their behavior is quite similar and linear. However, the HIFU transducer has worse results than the air-backing transducer, and the percentage of loss is similar to what you would expect, so there is not much benefit in using it.

It is worth mentioning that the envelopes of the HIFU transducer measurements have shown lower pressure values than the air-backing transducer because in order to get the same number of pulses in a wave, it was necessary to move the transducer away inside the tank. Since the HIFU transducer is focused, the hydrophone received less intensity, and therefore the pressure values were lower. However, this difference does not influence the results, as all the data was normalized, and a relative comparison was done in the percentage of loss as pulses were removed from the same transducer.

There are two possible explanations for the fact that the HIFU transducer has proven to be less beneficial than the air-backing transducer. The first possibility is that the HIFU transducer has a lower quality factor than the air-backing transducer. As mentioned in Chapter 2, with a high-quality factor, it is possible to achieve maximum ultrasound power when operated exactly at the resonance frequency. Having a transducer with a high-quality factor is a great advantage because it has a low power consumption, which is desired in this project. Another reason that might explain the higher loss in the HIFU transducer compared to the air-backing transducer is that the air-backing transducer has an air gap, as can be seen in **Figure 3.7**. This air gap allows the PZT to be free to resonate and vibrate more so it will oscillate after the pulse is removed instead of absorbing all the energy. Therefore, the percentage of loss is expected to be lower.

Through the graph from **Figure 4.19**, it is possible to conclude that the percentage of pulses to be removed in order to obtain the best result is about 20%. When 20% of the pulses were removed from the waveform, only 7% of the energy was lost. If 20% of energy is removed, it is expected to lose 20% of energy as well, however only 7% was lost, thus saving 13% of energy in this situation.

Based on the results shown in **Figure 4.20**, it can be seen that removing a percentage of the pulses instead of removing them completely is quite beneficial. It can be seen in the figure that the percentage of loss is greater when the pulses are completely removed, compared to when 50% of their amplitude is removed, and finally when only 30% of their amplitude is removed. All of the above cases proved to be beneficial in using less energy. However, removing only 30% of the pulse amplitude saves about 10 times more energy than removing the pulses completely.

It is important to point out that these measurements, although already simulated on the optical table, were subject to some measurement errors, just like the previous measurements. Here, the main error is due to the impedance that long cables bring, and also to less favorable weather conditions, such as wind. Although the measurements were made in the laboratory, any small airflow could cause the distilled water in the tank to move and interfere with the data acquisition.

5.3 EXPERIMENTAL SETUP OPEN CIRCUIT

The fourth goal of this thesis project was to see if there were significant differences that would positively influence the results when using an open circuit instead of a short circuit. Whenever a pulse was removed in the previous cases (short circuit), the PZT was forced to zero. Thus, as mentioned earlier, a way was created so that the PZT was not forced to zero, but simply to allow the PZT to oscillate freely when a pulse was removed (open circuit).

Figure 4.21 shows the results of the open circuit simulations. Unfortunately, as can be seen from the figure, the percentage of loss of these simulations proved not to be beneficial, as it was always higher than expected. When there is more energy lost than energy that was not sent, the results are not beneficial, and this is not what was intended with this project.

With this setup and simulation, measurement errors have increased significantly. All the possible errors associated with the cables mentioned above were multiplied because more cables and other electronic components were used, which are liable to noise. As can be seen in **Figure 3.18**, the PCB contained several capacitors, diodes, and interconnections where impedance could be amplified. Furthermore, instead of the cables being connected directly to the transducer, in this simulation, the cables were connected first to the PCB and only then to the transducer. In addition, a signal generator was used in these measurements, which is also subject to errors.

5.4 SHORT CIRCUIT VS OPEN CIRCUIT

Figure 4.22 shows the comparison between open and short circuits. As mentioned earlier, the open circuit simulations have not proven at all effective in saving energy. In this comparison, it is possible to interpret this result, and also conclude that the simulation through the short circuit is more efficient in comparison an open circuit simulation when it comes to saving energy.

In this image, although the short circuit simulation shows better results than the open circuit one, it should be mentioned that the short circuit result is not as good as desirable because it is done with the HIFU transducer, which as mentioned above is not very effective.

6 Conclusion

Ultrasound (US) Neuromodulation is a growing field in the neuroscience area, although its mechanisms are poorly understood which is an important obstacle to overcome for further progress. There is still a long way to go before US neuromodulation can be used to treat neurological conditions but there are high expectations of this technique.

In the past ten years, researchers have discovered an increased number of ultrasound bioeffects, expanding its potential clinical application. It is fascinating to observe how new therapeutic applications, such as neuromodulation and tissue ablation are being made possible through ultrasound, which has traditionally been used for diagnostic purposes, such as ultrasound imaging.

There are some factors that need to be taken into account before starting the usage of US neuromodulation to treat some diseases. Firstly, the instrumentation needs to be updated and improved to ensure the safety of humans and to improve the penetration depth. Most of the published research on current US neuromodulation systems was conducted on animals, and since they have smaller sizes of the brain and skull, here there are less problems with penetration depth. The ability to penetrate the human skull at a lower frequency (less than 1 MHz) comes at the sacrifice of spatial resolution.

In this study, we investigated whether it is possible to save energy during US neuromodulation by removing pulses from the waveform or by reducing their amplitude. Thus making it possible to manufacture portable equipment capable of performing ultrasonic neuromodulation. Our results suggest that some energy can be saved through acoustic wave pulse removal.

While using the air-backed transducer the results were more promising, and by removing about 20% of the input energy resulted in only about 7% of output loss, which is a considerable saving of energy. This result is very exciting since in this case about 13% of energy can be saved, which is quite considerable, and it is in agreement with the hypothesis presented in this study. By proving that a reasonable amount of energy can be saved, we are closer to being able to reduce the power consumption of ultrasound neuromodulation systems towards efficient battery power operation systems. With these systems, it will be possible to carry out treatment twenty-four hours a day, seven days a week through wearable devices.

On the other hand, the high-intensity focused ultrasound transducer was not as effective, and the percentage of energy loss in all simulations was very close to what could be expected, i.e., when it is removed 10% of the pulses it is expected the wave to lose 10% of its energy.

Regarding the air-backing transducer results, another very favorable conclusion was drawn from the simulations. The experiments where only a percentage of the pulse amplitude was removed, have shown better results than removing the pulses entirely, and among the results presented, removing 30% of the amplitude is the case with the lowest percentage of loss and therefore the highest efficiency.

Another comparison made in this dissertation suggests that performing pulse removal via a short circuit is quite favorable while performing pulse removal through an open circuit was less so, where no energy

saving was obtained. It should be noted that all these results entailed some measurement errors, nonetheless, the conclusions were clear and corroborated by each other. Therefore, this study opens an innovative investigation possibility and may then contribute to the evolution, and development of US neuromodulation in a more portable way, i.e., it may shed new light on treating neuronal diseases.

6.1 FUTURE WORK

There were some things that could have been done to improve this study, however, due to the shortage of time and material it was not possible to accomplish them. Firstly, all the results should have had a larger sample size in order to be more accurate. Another important thing was to reduce the measurement errors by, for example, using shorter cable lengths and by using the air table from the beginning. It is also worth mentioning that an impedance analysis was made for the air backing transducer in order to find out exactly what the resonance frequency was, but it wasn't performed for the HIFU transducer since it was a commercially obtained device, and the resonance frequency was designed and calibrated by external parties.

Future work must include experiments and simulations with neurons, either in mice or in living cells, since the behavior of ultrasound in neurons is still largely unknown and the results may prove to be either even more effective or not effective at all, so it is crucial to perform these experiments. Something to consider is also to use transducers with a higher quality factor and ensure that the simulation is performed at the resonance frequency since it is possible to achieve maximum US power and low power consumption with a high-quality factor. Future work also should include experiments to test whether reducing the energy required for treatment also reduces side effects and has the same medical efficiency.

References

[1] R.A. Novelline, *Squire's Fundamentals of Radiology 6th ed*. Harvard University Press Boston , 2004.

[2] Thomas Szabo, *Diagnostic Ultrasound Imaging: Inside Out*, 1st Edition. Burlington: MA: Elsevier Academic Press, 2004.

[3] FDA, "Marketing Clearance of Diagnostic Ultrasound Systems and Transducers," Jun. 2019.

[4] W. J. Tyler, Y. Tufail, M. Finsterwald, M. L. Tauchmann, E. J. Olson, and C. Majestic, "Remote excitation of neuronal circuits using low-intensity, low-frequency ultrasound," *PLoS One*, vol. 3, no. 10, Oct. 2008, doi: 10.1371/journal.pone.0003511.

[5] N. Zangiabadi, L. D. Ladino, F. Sina, J. P. Orozco-Hernández, A. Carter, and J. F. Téllez-Zenteno, "Deep Brain Stimulation and Drug-Resistant Epilepsy: A Review of the Literature," *Front Neurol*, vol. 10, Jun. 2019, doi: 10.3389/fneur.2019.00601.

[6] J. M. Stilling, O. Monchi, F. Amoozegar, and C. T. Debert, "Transcranial Magnetic and Direct Current Stimulation (TMS/tDCS) for the Treatment of Headache: A Systematic Review," *Headache: The Journal of Head and Face Pain*, vol. 59, no. 3, pp. 339–357, Mar. 2019, doi: 10.1111/head.13479.

[7] A. I. Sonmez *et al.*, "Accelerated TMS for Depression: A systematic review and meta-analysis," *Psychiatry Res*, vol. 273, pp. 770–781, Mar. 2019, doi: 10.1016/j.psychres.2018.12.041.

[8] H. Thair, A. L. Holloway, R. Newport, and A. D. Smith, "Transcranial Direct Current Stimulation (tDCS): A Beginner's Guide for Design and Implementation," *Front Neurosci*, vol. 11, Nov. 2017, doi: 10.3389/fnins.2017.00641.

[9] S. Yoo, D. R. Mittelstein, R. Hurt, J. Lacroix, and M. G. Shapiro, "Focused ultrasound excites neurons via mechanosensitive calcium accumulation and ion channel amplification", doi: 10.1101/2020.05.19.101196.

[10] G. ter Haar, "Therapeutic ultrasound," 1999. doi: doi: 10.1016/s0929-8266(99)00013-0.

[11] H. Baek, K. J. Pahk, and H. Kim, "A review of low-intensity focused ultrasound for neuromodulation," *Biomedical Engineering Letters*, vol. 7, no. 2. Springer Verlag, pp. 135–142, May 01, 2017. doi: 10.1007/s13534-016-0007-y.

[12] G. Pinton, J. F. Aubry, E. Bossy, M. Muller, M. Pernot, and M. Tanter, "Attenuation, scattering, and absorption of ultrasound in the skull bone," *Med Phys*, vol. 39, no. 1, pp. 299–307, 2012, doi: 10.1118/1.3668316.

[13] J. Kubanek, J. Shi, J. Marsh, D. Chen, C. Deng, and J. Cui, "Ultrasound modulates ion channel currents," *Sci Rep*, vol. 6, Apr. 2016, doi: 10.1038/srep24170.

[14] M. L. Prieto, K. Firouzi, B. T. Khuri-Yakub, and M. Maduke, "Activation of Piezo1 but Not NaV1.2 Channels by Ultrasound at 43 MHz," *Ultrasound Med Biol*, vol. 44, no. 6, pp. 1217–1232, Jun. 2018, doi: 10.1016/j.ultrasmedbio.2017.12.020.

[15] Z. Qiu *et al.*, "The Mechanosensitive Ion Channel Piezo1 Significantly Mediates In Vitro Ultrasonic Stimulation of Neurons," *iScience*, vol. 21, pp. 448–457, Nov. 2019, doi: 10.1016/j.isci.2019.10.037.

[16] H. A. S. Kamimura, A. Conti, N. Toschi, and E. E. Konofagou, "Ultrasound neuromodulation: Mechanisms and the potential of multimodal stimulation for neuronal function assessment," *Frontiers in Physics*, vol. 8. Frontiers Media S.A., pp. 1–9, May 01, 2020. doi: 10.3389/fphy.2020.00150.

[17] D. Dalecki, "Mechanical bioeffects of ultrasound," *Annual Review of Biomedical Engineering*, vol. 6. pp. 229–248, 2004. doi: 10.1146/annurev.bioeng.6.040803.140126.

[18] S. M. Thompson, L. M. Masukawa, and D. A. Prince, "Temperature Dependence of Intrinsic Membrane Properties and Synaptic Potentials in Hippocampal CA1 Neurons In Vitro'," 1985.

[19] M. G. Shapiro, K. Homma, S. Villarreal, C. P. Richter, and F. Bezanilla, "Infrared light excites cells by changing their electrical capacitance," *Nat Commun*, vol. 3, 2012, doi: 10.1038/ncomms1742.

[20] M. Plaksin, E. Shapira, E. Kimmel, and S. Shoham, "Thermal Transients Excite Neurons through Universal Intramembrane Mechanoelectrical Effects," *Phys Rev X*, vol. 8, no. 1, Mar. 2018, doi: 10.1103/PhysRevX.8.011043.

[21] M. Plaksin, S. Shoham, and E. Kimmel, "Intramembrane cavitation as a predictive bio-piezoelectric mechanism for ultrasonic brain stimulation," *Phys Rev X*, vol. 4, no. 1, 2014, doi: 10.1103/PhysRevX.4.011004.

[22] T. Zhang, N. Pan, Y. Wang, C. Liu, and S. Hu, "Transcranial Focused Ultrasound Neuromodulation: A Review of the Excitatory and Inhibitory Effects on Brain Activity in Human and Animals," *Front Hum Neurosci*, vol. 15, Sep. 2021, doi: 10.3389/fnhum.2021.749162.

[23] S. Wang *et al.*, "Ultrasonic Neuromodulation and Sonogenetics: A New Era for Neural Modulation," *Frontiers in Physiology*, vol. 11. Frontiers Media S.A., Jul. 16, 2020. doi: 10.3389/fphys.2020.00787.

[24] J. Blackmore, S. Shrivastava, J. Sallet, C. R. Butler, and R. O. Cleveland, "Ultrasound Neuromodulation: A Review of Results, Mechanisms and Safety," *Ultrasound in Medicine and Biology*, vol. 45, no. 7. Elsevier USA, pp. 1509–1536, Jul. 01, 2019. doi: 10.1016/j.ultrasmedbio.2018.12.015.

[25] D. Maresca *et al.*, "Biomolecular Ultrasound and Sonogenetics," 2018, doi: 10.1146/annurev-chembioeng.

[26] Y. Yuan, Z. Wang, M. Liu, and S. Shoham, "Cortical hemodynamic responses induced by low-intensity transcranial ultrasound stimulation of mouse cortex," *Neuroimage*, vol. 211, p. 116597, May 2020, doi: 10.1016/j.neuroimage.2020.116597.

[27] S.-S. Yoo *et al.*, "Focused ultrasound modulates region-specific brain activity," *Neuroimage*, vol. 56, no. 3, pp. 1267–1275, Jun. 2011, doi: 10.1016/j.neuroimage.2011.02.058.

[28] Y. Yuan, J. Yan, Z. Ma, and X. Li, "Effect of noninvasive focused ultrasound stimulation on gamma oscillations in rat hippocampus," *Neuroreport*, vol. 27, no. 7, pp. 508–515, May 2016, doi: 10.1097/WNR.0000000000000572.

[29] M. E. Moore, J. M. Loft, W. C. Clegern, and J. P. Wisor, "Manipulating neuronal activity in the mouse brain with ultrasound: A comparison with optogenetic activation of the cerebral cortex," *Neurosci Lett*, vol. 604, pp. 183–187, Sep. 2015, doi: 10.1016/j.neulet.2015.07.024.

[30] E. Mehić, J. M. Xu, C. J. Caler, N. K. Coulson, C. T. Moritz, and P. D. Mourad, "Increased Anatomical Specificity of Neuromodulation via Modulated Focused Ultrasound," *PLoS One*, vol. 9, no. 2, p. e86939, Feb. 2014, doi: 10.1371/journal.pone.0086939.

[31] G. Li *et al.*, "Noninvasive Ultrasonic Neuromodulation in Freely Moving Mice," *IEEE Trans Biomed Eng*, vol. 66, no. 1, pp. 217–224, Jan. 2019, doi: 10.1109/TBME.2018.2821201.

[32] C. Aurup, H. A. S. Kamimura, and E. E. Konofagou, "High-Resolution Focused Ultrasound Neuromodulation Induces Limb-Specific Motor Responses in Mice in Vivo," *Ultrasound Med Biol*, vol. 47, no. 4, pp. 998–1013, Apr. 2021, doi: 10.1016/j.ultrasmedbio.2020.12.013.

[33] H. Kim *et al.*, "Miniature ultrasound ring array transducers for transcranial ultrasound neuromodulation of freely-moving small animals," *Brain Stimul*, vol. 12, no. 2, pp. 251–255, Mar. 2019, doi: 10.1016/j.brs.2018.11.007.

[34] W. Lee *et al.*, "Image-Guided Focused Ultrasound-Mediated Regional Brain Stimulation in Sheep," *Ultrasound Med Biol*, vol. 42, no. 2, pp. 459–470, Feb. 2016, doi: 10.1016/j.ultrasmedbio.2015.10.001.

[35] J. A. Cain *et al.*, "Ultrasonic thalamic stimulation in chronic disorders of consciousness," *Brain Stimul*, vol. 14, no. 2, pp. 301–303, Mar. 2021, doi: 10.1016/j.brs.2021.01.008.

[36] P. P. Ye, J. R. Brown, and K. B. Pauly, "Frequency Dependence of Ultrasound Neurostimulation in the Mouse Brain," *Ultrasound Med Biol*, vol. 42, no. 7, pp. 1512–1530, Jul. 2016, doi: 10.1016/j.ultrasmedbio.2016.02.012.

[37] J. L. Sanguinetti *et al.*, "Transcranial Focused Ultrasound to the Right Prefrontal Cortex Improves Mood and Alters Functional Connectivity in Humans," *Front Hum Neurosci*, vol. 14, Feb. 2020, doi: 10.3389/fnhum.2020.00052.

[38] A. Fomenko *et al.*, "Systematic examination of low-intensity ultrasound parameters on human motor cortex excitability and behavior," *Elife*, vol. 9, Nov. 2020, doi: 10.7554/eLife.54497.

[39] S. Hameroff *et al.*, "Transcranial Ultrasound (TUS) Effects on Mental States: A Pilot Study," *Brain Stimul*, vol. 6, no. 3, pp. 409–415, May 2013, doi: 10.1016/j.brs.2012.05.002.

[40] W. Legon, L. Ai, P. Bansal, and J. K. Mueller, "Neuromodulation with single-element transcranial focused ultrasound in human thalamus," *Hum Brain Mapp*, vol. 39, no. 5, pp. 1995–2006, May 2018, doi: 10.1002/hbm.23981.

[41] B. C. Gibson *et al.*, "Increased Excitability Induced in the Primary Motor Cortex by Transcranial Ultrasound Stimulation," *Front Neurol*, vol. 9, Nov. 2018, doi: 10.3389/fneur.2018.01007.

[42] W. Lee *et al.*, "Transcranial focused ultrasound stimulation of human primary visual cortex" *Sci Rep*, vol. 6, no. 1, p. 34026, Sep. 2016, doi: 10.1038/srep34026.

[43] J. A. Cain *et al.*, “Real time and delayed effects of subcortical low intensity focused ultrasound,” *Sci Rep*, vol. 11, no. 1, p. 6100, Dec. 2021, doi: 10.1038/s41598-021-85504-y.

[44] Paris Brain Institute, “OCD - OBSESSIVE COMPULSIVE DISORDERS,” 2022.

[45] Lindsay Modglin, “Single Care- Epilepsy statistics 2022,” *https://www.singlecare.com/blog/news/epilepsy-statistics/*, 2022.

[46] World Health Organization, “Depression,” *https://www.who.int/news-room/fact-sheets/detail/depression*, Sep. 13, 2021.

[47] Y. Chen *et al.*, “Ultrasound Neuromodulation: Integrating Medicine and Engineering for Neurological Disease Treatment,” *BIO Integration*, vol. 2, no. 4, pp. 169–179, Dec. 2021, doi: 10.15212/bioi-2020-0026.

[48] National Health Service United Kingdom, “Overview: Epilepsy,” *https://www.nhs.uk/conditions/epilepsy/*, Sep. 18, 2020.

[49] W. H. Theodore and R. S. Fisher, “Brain stimulation for epilepsy,” *Lancet Neurol*, vol. 3, no. 2, pp. 111–118, Feb. 2004, doi: 10.1016/S1474-4422(03)00664-1.

[50] R. Fisher *et al.*, “Electrical stimulation of the anterior nucleus of thalamus for treatment of refractory epilepsy,” *Epilepsia*, vol. 51, no. 5, pp. 899–908, May 2010, doi: 10.1111/j.1528-1167.2010.02536.x.

[51] National institute of Aging- United States, “Alzheimer’s Disease Fact Sheet,” *https://www.nia.nih.gov/health/alzheimers-disease-fact-sheet*.

[52] A. R. Marks, “In search of memory The emergence of a new science of mind,” *Journal of Clinical Investigation*, vol. 116, no. 5, pp. 1131–1131, May 2006, doi: 10.1172/JCI28674.

[53] G. I. Papakostas, “Tolerability of modern antidepressants.,” *J Clin Psychiatry*, vol. 69 Suppl E1, pp. 8–13, 2008.

[54] F. Fregni, P. S. Boggio, M. A. Nitsche, M. A. Marcolin, S. P. Rigonatti, and A. Pascual-Leone, “Treatment of major depression with transcranial direct current stimulation,” *Bipolar Disord*, vol. 8, no. 2, pp. 203–204, Apr. 2006, doi: 10.1111/j.1399-5618.2006.00291.x.

[55] M. S. George *et al.*, “Daily repetitive transcranial magnetic stimulation (rTMS) improves mood in depression,” *Neuroreport*, vol. 6, no. 14, pp. 1853–1856, Oct. 1995, doi: 10.1097/00001756-199510020-00008.

[56] H. S. Mayberg *et al.*, “Deep Brain Stimulation for Treatment-Resistant Depression,” *Neuron*, vol. 45, no. 5, pp. 651–660, Mar. 2005, doi: 10.1016/j.neuron.2005.02.014.

[57] National Institute of Aging - United States, “Parkinson’s Disease: Causes, Symptoms, and Treatments,” *https://www.nia.nih.gov/health/parkinsons-disease*, Apr. 14, 2022.

[58] P. Limousin, J. D. Speelman, F. Gielen, M. Janssens, and study collaborators, “Multicentre European study of thalamic stimulation in parkinsonian and essential tremor,” *J Neurol Neurosurg Psychiatry*, vol. 66, no. 3, pp. 289–296, Mar. 1999, doi: 10.1136/jnnp.66.3.289.

[59] J. M. Bronstein *et al.*, “Deep Brain Stimulation for Parkinson Disease,” *Arch Neurol*, vol. 68, no. 2, Feb. 2011, doi: 10.1001/archneurol.2010.260.

[60] Y. Yuan, J. Yan, Z. Ma, and X. Li, “Effect of noninvasive focused ultrasound stimulation on gamma oscillations in rat hippocampus,” *Neuroreport*, vol. 27, no. 7, pp. 508–515, May 2016, doi: 10.1097/WNR.0000000000000572.

[61] L. Longley, “Anaesthesia and analgesia in rabbits and rodents,” *In Pract*, vol. 30, no. 2, pp. 92–97, Feb. 2008, doi: 10.1136/inpract.30.2.92.

[62] Y. Younan, T. Deffieux, B. Larrat, M. Fink, M. Tanter, and J.-F. Aubry, “Influence of the pressure field distribution in transcranial ultrasonic neurostimulation,” *Med Phys*, vol. 40, no. 8, p. 082902, Jul. 2013, doi: 10.1118/1.4812423.

[63] W. Lee *et al.*, “Transcranial focused ultrasound stimulation of human primary visual cortex,” *Sci Rep*, vol. 6, no. 1, p. 34026, Sep. 2016, doi: 10.1038/srep34026.

[64] J. M. Stern *et al.*, “Safety of focused ultrasound neuromodulation in humans with temporal lobe epilepsy,” *Brain Stimul*, vol. 14, no. 4, pp. 1022–1031, Jul. 2021, doi: 10.1016/j.brs.2021.06.003.

[65] M. K. Feldman, S. Katyal, and M. S. Blackwood, “US Artifacts,” *RadioGraphics*, vol. 29, no. 4, pp. 1179–1189, Jul. 2009, doi: 10.1148/rg.294085199.

[66] Anant Agarwal and Jeffrey H. Lang, *Foundations of Analog and Digital Electronic Circuits.Department of Electrical Engineering and Computer Science*. Massachusetts Institute of Technology, 2005.

[67] E. Sassaroli and N. Vykhodtseva, “Acoustic neuromodulation from a basic science prospective,” *J Ther Ultrasound*, vol. 4, no. 1, p. 17, Dec. 2016, doi: 10.1186/s40349-016-0061-z.

[68] X. Chen *et al.*, “Piezoelectric micromachined ultrasonic transducers with low thermoelastic dissipation and high quality factor,” *Journal of Micromechanics and Microengineering*, vol. 28, no. 5, p. 057001, May 2018, doi: 10.1088/1361-6439/aab1bc.

[69] *Structural Health Monitoring (SHM) in Aerospace Structures*. Elsevier, 2016. doi: 10.1016/C2014-0-00994-X.

[70] Z. Zhang *et al.*, “Design and comparison of PMN-PT single crystals and PZT ceramics based medical phased array ultrasonic transducer,” *Sens Actuators A Phys*, vol. 283, pp. 273–281, Nov. 2018, doi: 10.1016/j.sna.2018.09.067.

[71] Oleg D Neikov, Stanislav Naboychenko, Irina B Mourachova, Victor G Gopienko, Irina V Frishberg, and Dina V Lotsko, *Handbook of Non-Ferrous Metal Powders Technologies and Applications*, Second edition. 2019.

[72] M. Vladimir and S. Vladimir, “Optical tables vibration isolation during precision measurements,” in *Procedia Engineering*, 2015, vol. 111, pp. 561–568. doi: 10.1016/j.proeng.2015.07.043.

Appendix

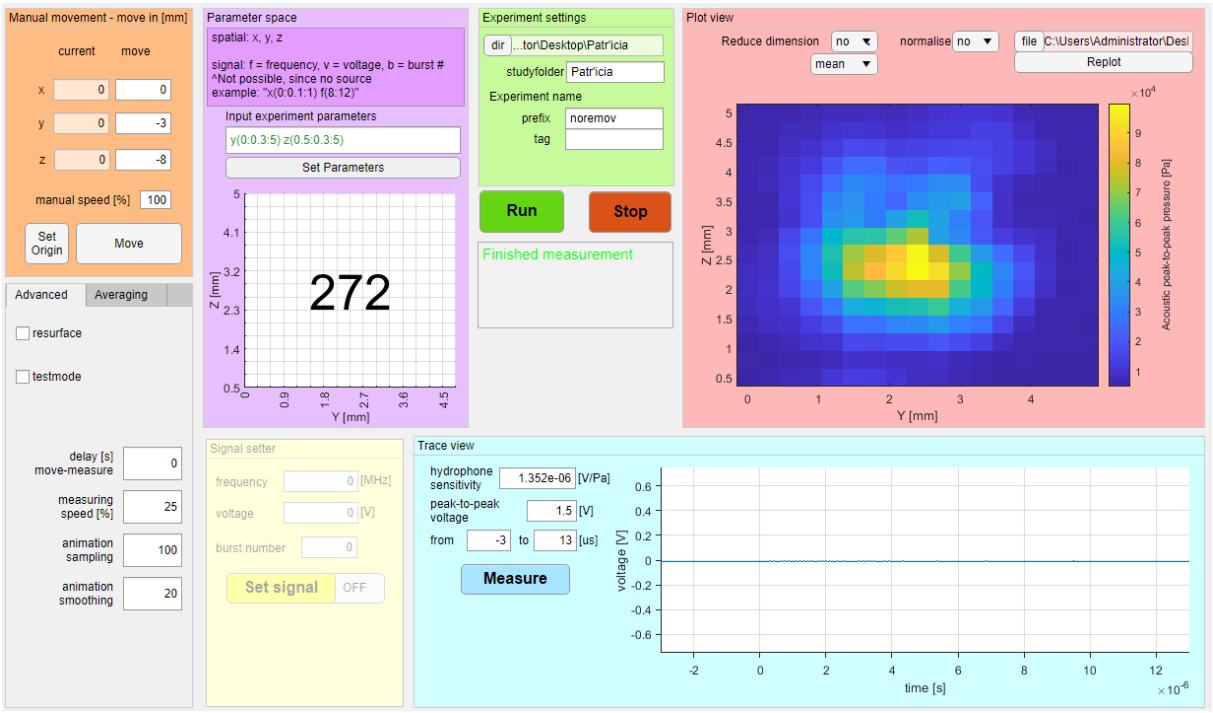

Figure A.1 *– Layout of the Experiment Visual Acoustics, EVA*